PFC/JA-89-6

Neoclassical Transport of Isotropic Fast Ions

Hsu, C.T., Catt, P.J., and Sigmar, D.J.

Plasma Fusion Center
Massachusetts Institute of Technology
Cambridge, MA 02139

February 1989

Submitted to: Physics of Fluids

This work was supported by the U. S. Department of Energy Contract No. DE-AC02-78ET51013. Reproduction, translation, publication, use and disposal, in whole or in part by or for the United States government is permitted.

Neoclassical Transport Of Isotropic Fast Ions

C. T. Hsu[1], P. J. Catto[2]

and D. J. Sigmar[1]

[1] *Massachusetts Institute of Technology, Cambridge, MA, USA*

[2] *Lodestar Research Corporation, Boulder, CO, USA*

Abstract

A study of the radial gradients driven neoclassical transport for fast ions, produced by isotropic source, in an axisymmetric toroidal system is present. The governing equation, the bounce averaged Fokker-Planck equation which contains both effects of the pitch angle scattering and the drag, is solved by utilizing the eigenfunction technique in cooperation with a rigorous numerical treatment. The results, which contain the complete physics of both collisional effects for finite inverse-aspect-ratio ($\epsilon \equiv \frac{r}{R_o}$), are found to be, for most of the relevant parameter regimes, in between of the previous limiting calculations[1,4].

I. Introduction

The radial losses of the energetic ions produced from an isotropic source are of special interest regarding their role to maintain ignition in an fusing plasma system. Originally[1], these losses were evaluated by keeping only drag in the collision operator. The resulting fluxes were therefore found to be only due to the decrease in the radial excursions of the trapped energetic ions as they slowed down by drag, an effect sometime refered to as 'banana collapse'. Since the neglection of the pitch angle scattering is not obvious, several efforts[2-4] have been made recently to retain the effects of pitch angle scattering for evaluating these radial transport fluxes. However, all these recent treatments, which, in contrast to Ref. [1], emphasized only the pitch angle scattering terms in the collision operator when solving for the fast ions distribution function, are also incomplete. In particular, in Ref. [4], an attempt to include both contributions from the drag and the pitch angle scattering was made, but, inconsistently, the distribution function associated with the pitch angle scattering only was used.

In the presence of both the drag and the pitch angle scattering, a fast ion will suffer both collisional effects during the slowing down process. Usually, it suffers more drag at birth, then, more and more pitch angle scattering than drag as it is slowed down due to the drag. One can therefore roughly categorize the fast particles into three classes in the velocity space — (i) which suffer mostly the pitch angle scattering, (ii) which suffers mostly the drag forces, (iii) which suffer both collisional effects in the same order of magnitude. It is found in this work that there are three distinct contributions to the radial transport losses corresponding to each class of particles. As for which contribution is more important, one needs to specify several physical parameters such as the birth velocity of fast ions, the critical velocity above which the electron drag is dominating, and the inverse aspect ratio. Combined, they can determine the fraction of each class of particles in velocity space, and the possibility for pitch angle scattering to detrap the trapped fast ions. In particular, the finite aspect ratio effects are especially important since each class of particles has transport fluxes with different scaling in ϵ. The detailed analysis of this argument will be given in the rest of this work.

Mathematically, as will be pointed out in Sec. II, both limits adopted in the previous works[1,4] are singular limits to the real system; therefore, it is important for the present work to carefully retain the complete physics of pitch angle scattering and drag, for arbitrary ϵ. Since the governing equation for the solution of distribution function, the bounce-averaged Fokker-Planck equation, is a 2-D inhomogeneous partial differential equation, we adopt the eigenfunction technique[5] in order to reduce it to an eigenfunction equation for the pitch angle operator and an inhomogeneous ordinary differential equation for the slowing down operator. Consequently, the radial fluxes with complete physics can be determined upon rigorously solving for the eigensolutions. Quantitatively, for most typical parameters in fusing tokomak plasmas, our results are found to be much larger than those in Ref. [1] but smaller than in Ref. [4].

As in most of the neoclassical transport theory of the magnetized plasma we assume $\delta_p \equiv \frac{\rho_p}{L}$ (where ρ_p is the poloidal gyroradius and L the radial scale length) to be a small quantity, and then utilize it as an expansion parameter. That is, the present work is not adequate for evaluating the transport fluxes of fast ions with banana width comparable to the length scale. In addition, we restrict ourselve to the axisymmetric system and with isotropic source. For instance, our calculations are inadequate for radial transport of fast ions produced from NBI if the source is anisotropic in velocity space.

In section II, a theoretical formulation which leads to the bounce-averaged Fokker-Planck equation and the general form of radial transport fluxes are given, in cooporation with the eigenfunction expansion. In section III, the solutions will be determined, both numerically for finite ϵ and analytically with perturbation theory for small ϵ. Discussions and comparisons of the results with that of the previous calculations will also be given. Section IV contains a summary of the results, a detailed discussion of the physical mechanisms causing the transport in various regions of velocity space and final remarks about extensions of this work to transport of energetic ions with finite banana width.

II. Theoretical Formulation

To describe the collisional behavior of the fast ions in an axisymmetric toroidal system, the procedure, which first derives the bounce-averaged Fokker-Planck equation and then solves it with an eigenfunction technique by utilizing the self-adjoint property of the pitch angle scattering operator, has been previously developed. In this section, we review this procedure to yield the distribution function and hence the neoclassical transport for fast ions with isotropic source. For further details, we refer readers to Refs. [4,5].

A. Bounce Averaged Fokker-Planck Equation

Considering the fast-ion species with isotropic source S (e.g., for D-T fusion, $S = n_D n_T \langle \sigma_f v \rangle$) and birth speed v_o, the kinetic equation is

$$\dot{f} = C(f) + \frac{S}{4\pi v^2}\delta(v - v_o) \; . \tag{1}$$

Here, $\dot{f}$ is the Vlasov operator and $C(f)$ the Fokker-Planck collision operator. For $v_i \ll v \ll v_e$, where v is fast ion particle speed and v_i, v_e are the thermal speeds of the Maxwellian background ions and electrons, $C(f)$ has the approximated form[6]

$$C(f) = \frac{1}{\tau_s}\frac{\partial}{\partial \vec{v}} \cdot \left[\left(1 + \frac{v_c^3}{v^3}\right)\vec{v}f + \frac{v_b^3}{2v^3}\left(v^2 \overleftrightarrow{I} - \vec{v}\vec{v}\right) \cdot \frac{\partial}{\partial \vec{v}} f \right] \tag{2}$$

with

$$v_c^3 = \left[3\pi^{1/2} T_e^{3/2} \sum_j (Z_j^2 N_j \ln \Lambda_j / m_j) \right] \Big/ \left[(2m_e)^{1/2} N_e \ln \Lambda_e \right] \; ,$$

$$v_b^3 = \left[3\pi^{1/2} T_e^{3/2} \sum_j (Z_j^2 N_j \ln \Lambda_j) \right] \Big/ \left[(2m_e)^{1/2} N_e m \ln \Lambda_e \right] \; ,$$

and

$$\tau_s \equiv 3m T_e^{3/2} \Big/ \left[4(2\pi m_e)^{1/2} Z^2 e^4 N_e \ln \Lambda_e \right] \; .$$

In the preceding, m_j, Z_j, N_j and $ln\Lambda_j$ are the mass, density, charge and Coulomb logarithm for species j, and the quantities without the subscript correspond to the fast ion

species. Here, the self collisions of the fast ion species are neglected due to the smallness of its density, so the sums in v_c^3 and v_b^3 are over all the thermalized background ion species only. The parameters τ_s and v_c are the slowing down time associated with electron drag and the speed above which electron drag dominates over ion drag. The speed v_b characterizes pitch angle scattering of the fast ions by the thermalized background ions so that the deflection time is $\frac{\tau_s v^3}{2v_b^3}$. For the energetic alpha particles immersed in background ions with equal amounts of deuterium and tritium, $\frac{v_b^3}{v_c^3} = \frac{3}{5}$.

Following Ref.[4], we expand Eq. (1) in δ_p, i.e., $f = f_o + f_1 + \cdots$. Then, we solve for the lowest order solution f_o, i.e.,

$$f_o = \frac{S\tau_s}{4\pi(v^3 + v_c^3)} H(v_o - v) \tag{3}$$

which is a consequence of the balance between the isotropic source and the drag portion of collision operator. We then gyrophase-average over the first order equation and obtain

$$v_\parallel \vec{b} \cdot \vec{\nabla} \left(\overline{f}_1 + \frac{I}{\Omega} v_\parallel \frac{\partial}{\partial \psi} f_o \bigg|_E \right) = \overline{C}(\overline{f}_1). \tag{4}$$

Here $H(v_o - v)$ is the unit step function which vanishes for $v > v_o$, E is the energetic particle total energy, $\Omega \equiv \frac{ZeB}{mc}$ is the gyrofrequency and the overbar denotes gyrophase-average. The usual axisymmetric flux coordinate system (φ, ψ, θ), (the toroidal angle, the poloidal flux function, the poloidal angle), is adopted so that $\vec{B} = I\vec{\nabla}\varphi + \vec{\nabla}\varphi \times \vec{\nabla}\psi$, $\vec{B} \cdot \vec{\nabla} = \frac{1}{J}\frac{\partial}{\partial \theta}$, $J \equiv \left| \vec{\nabla}\varphi \times \vec{\nabla}\psi \cdot \vec{\nabla}\theta \right|^{-1}$, and for low beta plasma, $I = I(\psi)$. The gyrophase-averaged collision operator has the form

$$\overline{C}(g) = \frac{1}{\tau_s} \left\{ \frac{1}{v^2} \frac{\partial}{\partial v} \left[\left(v^3 + v_c^3\right) g \right] + \frac{2v_b^3}{v^3} h\xi \frac{\partial}{\partial \lambda} \lambda \xi \frac{\partial}{\partial \lambda} g \right\} \tag{5}$$

where, $\lambda \equiv \frac{v_\perp^2 h}{v^2}$, $\xi \equiv \frac{v_\parallel}{v} = \pm(1 - \frac{\lambda}{h})^{\frac{1}{2}}$, $h \equiv \frac{B_o}{B}$, B_o the magnetic field at the magnetic axis, and $\Omega_o \equiv \frac{ZeB_o}{mc}$.

It is important to emphasize here that the validity for the well-known slowing-down distribution f_o of Eq. (3), depends strongly on two assumptions we have made: (1) isotropic source, and (2) smallness of δ_p. When anisotropic source, (for instance, NBI), is considered, the pitch angle scattering effects become very important in zeroth order[5], and as a

consequence, $f_o = f_o(\psi, v, \lambda)$. For the case that $\delta_p \sim 0(1)$, the banana width $\Delta r_b \simeq \sqrt{\epsilon}\delta_p L$ becomes so large that the trapped particles suffer 0(1) difference in collisional forces on the banana trajectory[7], whence $f_o = f_o(\psi, \theta, v, \lambda)$ results. However, both of these effects are not included in this work.

By defining P, the localized part of the distribution function, such that

$$\overline{f}_1 = \left(\frac{-I}{2\Omega_o} v \frac{\partial}{\partial \psi} f_o \Big|_E\right) \left[2h\xi + P\right] \tag{6}$$

and exploiting that the bounce period τ_B is much shorter than the slowing-down time τ_s, one can further expand P in $\frac{\tau_B}{\tau_s}$ and finds that the lowest order of P in $\frac{\tau_B}{\tau_s}$ is independent of θ, i.e., satisfies $P = P(\psi, v, \lambda)$. In addition, as is well-known[8], due to rotational symmetry of the collision operator and particle conservation at the banana tips, one also concludes that $P = 0$ in the trapped region. The solubility condition of Eq. (4),

$$\left\langle \frac{B}{v_\parallel} \overline{C}(\overline{f}_1) \right\rangle = 0$$

thus yields the bounce-averaged equation for P

$$v_b^3 \left(\frac{\partial}{\partial \psi} f_o \Big|_E\right) \frac{\partial}{\partial \lambda} \lambda \left(1 - \langle \xi \rangle \frac{\partial}{\partial \lambda} P\right) = \frac{\partial}{\partial v} \left\{(v^3 + v_c^3) v \left(\frac{\partial}{\partial \psi} f_o \Big|_E\right) \left(1 - \frac{\partial \langle \xi \rangle}{\partial \lambda} P\right)\right\} \tag{7}$$

where the right-hand side describes the drag and the left-hand side describes the pitch angle scattering. Here,

$$\langle \cdots \rangle \equiv \oint \frac{d\theta}{2\pi} J(\cdots) \Big/ \oint \frac{d\theta}{2\pi} J$$

denotes the flux surface average.

In the next subsection, the inhomogeneous partial differential equation, Eq. (7), will be further separated into an inhomogeneous ordinary differential equation with respect to v and an eigenfunction equation with respect to λ. However, it is instructive to remark here that two limiting solutions of Eq. (7), (i) the "drag only" solution[1], P_d, and (ii) the "pitch angle scattering only" solution[2], P_{pa}, have been previously adopted to approximate the radial transport. Here,

$$P_d = \left(\frac{\partial < \xi >}{\partial \lambda}\right)^{-1} \tag{8a}$$

is deduced from Eq. (7) by taking v_b^3 to be zero and

$$\frac{\partial}{\partial\lambda}P_{pa} = \frac{1}{<\xi>} \tag{8b}$$

is deduced from Eq. (7) by taking v_b^3 to be ∞. Nonetheless, neither of them are relevant for describing the real solution. This is because (i) the $v_b = 0$ limit, which leads to the "drag only" solution P_d, is a singular limit with respect to the differential operator for λ; and (ii) the $v_b = \infty$ limit, which leads to the "pitch angle scattering only" solution P_{pa}, is a singular limit with respect to the differential operator for v.

B. The Eigenfunction Technique

Since the operators in Eq. (7) are separable in λ and v, and the pitch angle scattering operator is self-adjoint, following Ref. [5], one can express the solution P as a series of orthogonal eigenfunctions in the form

$$P(\psi, v, \lambda) = \sum_{n=1}^{\infty} \Lambda_n(\psi, \lambda) V_n(\psi, v) \tag{9a}$$

where Λ_n is the eigenfunction of the equation

$$\frac{\partial}{\partial\lambda}\lambda <\xi> \frac{\partial}{\partial\lambda}\Lambda_n = \kappa_n \frac{\partial <\xi>}{\partial\lambda}\Lambda_n \tag{10a}$$

with eigenvalue κ_n, satisfying the following boundary conditions:

$$\begin{cases} \text{at the passing boundary, } \lambda = 0, & \Lambda_n = 1, \\ \text{at the trapped-passing boundary, } \lambda \equiv \lambda_c = 1 - \epsilon, & \Lambda_n = 0, \end{cases} \tag{10b}$$

Before proceeding, it is useful to discuss the asymptotic behavior of the eigenfunctions Λ_n near both boundaries. Near the passing boundary, $\lambda \to 0$, since $<\xi> \to 1$, $\frac{\partial}{\partial\lambda}<\xi> \to -\frac{1}{2} < \frac{1}{h} >$ (i.e., a regular singular boundary), Eq. (10a) reduces to the eigenequation which generates the zeroth order Bessel functions, J_o and Y_o. Near the trapped-passing boundary, $\lambda \to \lambda_c$, since $\langle\xi\rangle \to \xi_t (\simeq \frac{2}{\pi}\sqrt{2\epsilon}$ for small ϵ) but $\frac{\partial}{\partial\lambda} <\xi>$ is logarithmically singular (i.e., an irregular singular boundary). Thus Eq. (10a) has two possible approximate solutions:

$\Lambda_n \propto \lambda^{\kappa_n}$ and $\frac{\partial \Lambda_n}{\partial \lambda} \propto \frac{1}{<\xi>}$. Only one solution for each boundary satisfies Eq. (10b), that is,

$$\begin{cases} \text{near the passing boundary,} & \Lambda_n \to J_o(\sqrt{2\lambda\langle\frac{1}{h}\rangle\kappa_n}) \simeq 1 - \frac{\lambda}{2}\langle\frac{1}{h}\rangle\kappa_n, \\ \text{near the trapped-passing boundary,} & \Lambda_n/\frac{\partial \Lambda_n}{\partial \lambda} \to - < \xi > \int_\lambda^{\lambda_c} d\lambda' \frac{1}{<\xi>} \ . \end{cases} \tag{10c}$$

It is now clear that the "drag only" solution P_d is an irrelevant solution as long as v_b is nonzero, no matter how small it is; because P_d is not able to satisfy the asymptotic behavior near the trapped-passing boundary.

The orthogonality property of Λ_n is

$$\int_o^{\lambda_c} d\lambda \ \Lambda_n \Lambda_m \frac{\partial < \xi >}{\partial \lambda} = 0 \ , \quad \text{for} \ \ m \neq n \ .$$

Also, it is worth mentioning that, due to the Sturm-Liouville form of Eq. (10a), the eigenvalue κ_n has a variational form

$$\kappa_n \left[\Lambda_n\right] = \frac{\int_o^{\lambda_c} d\lambda \ \lambda < \xi > (\frac{\partial}{\partial \lambda}\Lambda_n)^2}{-\int_o^{\lambda_c} d\lambda \ \frac{\partial <\xi>}{\partial \lambda}\Lambda_n^2} \tag{11}$$

and thus can be calculated variationally using a suitably constructed trial function. The absolute minimum of the variational functional is the lowest eigenvalue κ_1.

Utilizing the orthogonality of Λ_n, multiplying Eq. (7) by Λ_m and integrating over λ, one finds that V_n is the solution of the equation

$$\frac{\partial}{\partial v}\left[v\left(\frac{v^3+v_c^3}{v_b^3}\right)(\sigma_n - V_n)\right] + \frac{v^3+v_c^3}{v_b^3}(\sigma_n - V_n) v \frac{\partial}{\partial v}\left(\ln \frac{\partial f_o}{\partial \psi}\bigg|_E\right) = \sigma_n - \kappa_n V_n \tag{12a}$$

The boundary condition for V_n at $v = v_o$ becomes, considering Eq. (3),

$$V_n(\psi, v_o) = \sigma_n \left[\Lambda_n\right] \equiv \frac{\int_o^{\lambda_c} d\lambda \ \Lambda_n}{\int_o^{\lambda_c} d\lambda \ \frac{\partial <\xi>}{\partial \lambda}\Lambda_n^2} \tag{12b}$$

Again, one notices that, except for the special case that $\kappa_n = 1$, the $v_b^3 \to \infty$ limit leads to solution $V_n = \frac{\sigma_n}{\kappa_n}$ which violates the boundary condition Eq. (12b), obviously a singular limit for Eqs. (12).

By solving the inhomogeneous ordinary equation Eqs. (12), V_n is obtained rigorously as

$$V_n = \sigma_n \left\{ 1 - (\kappa_n - 1) \frac{v_b^3}{(v_c^3 + v^3) v \frac{\partial f_o}{\partial \psi}\Big|_E} \int_v^{v_o} du \left(\frac{v^3(v_c^3 + u^3)}{u^3(v_c^3 + v^3)} \right)^{\frac{\kappa_n v_b^3}{3 v_c^3}} \frac{\partial f_o(u)}{\partial \psi}\Big|_{E(u)} \right\} \quad (13)$$

Therefore P, the solution of Eq. (7), is completely determined upon solving for Λ_n, κ_n from the eigenequation Eq. (10a). For finite inverse-aspect ratio ϵ, Eq. (10a) should be solved numerically; while for $\epsilon \ll 1$, it can be approximately solved using perturbation analysis, carefully taking into account the trapped-passing boundary effects. These are given in Sec. III.

C. Neoclassical Transport Fluxes

By flux surface averaging over the $R^2 \nabla \varphi$ projection of the moment equations of momentum and heat flow, one obtains the well-known form for the neoclassical radial fluxes

$$\Gamma_{neo}^d = \frac{-I}{\Omega_o} \left\langle \int d\vec{v} \left(\frac{mv^2}{2} \right)^d v_\parallel h \overline{C}(\overline{f}_1) \right\rangle$$

which, by using Eqs. (3), (5) and (6), yields

$$\Gamma_{neo}^d = -\left(\frac{mv_o^2}{2} \right)^d \left(\frac{v_o I}{\Omega_o} \right)^2 S \sum_{l=1}^{2} (-1)^{l+1} A_l C_{d,l} \quad (14)$$

where superscript d denotes particle flux for $d = 0$ and heat flux for $d = 1$. Here, the normalized diffusion coefficients $C_{d,l}[P]$ are defined by

$$C_{d,l}[P] \equiv \frac{1}{3} \left(\frac{v_c}{v_o} \right)^{2d+2} \int_o^{v_o} \frac{dv}{v_c} \left\{ \left(\frac{v}{v_c} \right)^{2d+1} \frac{(\frac{v_b}{v_c})^3 + (2d+1)(1 + (\frac{v}{v_c})^3)}{(1 + (\frac{v}{v_c})^3)^l} \left[< h^2 > + \frac{3}{4} \int_o^{\lambda_c} P d\lambda \right] \right\} \quad (15)$$

with $A_1 \equiv \frac{\partial}{\partial \psi} \ln(S \tau_s)$, and $A_2 \equiv \frac{\partial}{\partial \psi} \ln(v_c^3)$. Hence the radial transport fluxes are determined upon correctly solving for P. Note that A_1 and A_2 are the radial gradient driving forces, and for fast ions produced in a fusing plasma, A_1 and A_2 are mainly corresponding

to the electron density and temperature profile. Also note that the radial electric force due to $\frac{\partial \phi}{\partial \psi}$ is neglected because, for fast ions, $\frac{Ze\phi}{mv_o^2} \ll 1$ can be assumed *a priori*. (In principle, $\frac{\partial \phi}{\partial \psi}$ can be determined from ambipolarity.)

Now, by using the eigenfunction expansion form of P, i.e., from Eqs. (9), (12), and (13), one is able to express the normalized diffusion coefficients, $C_{d,l}[P]$ in Eq. (15), in terms of eigenfunctions. On the other hand, from the fact that V_n in Eq. (13), and therefore $C_{d,l}[P]$ in Eq. (15), involves the radial gradients A_l, one notices that some rearrangements are needed to extract A_l out of $C_{d,l}$. After lengthy manipulations, one finds

$$\begin{aligned} C_{d,l} \equiv & Q_p \left[< h^2 > - \sum_{n=1}^{\infty} \frac{\Upsilon_n}{\kappa_n} \right] L_{d,l+1} + (2d+1) \left[< h^2 > - \sum_{n=1}^{\infty} \frac{\Upsilon_n}{\kappa_n} (2 - \frac{1}{\kappa_n}) \right] L_{d,l} \\ & - (2d+1) \sum_{n=1}^{\infty} \left[\Upsilon_n (1 - \frac{1}{\kappa_n})^2 I_{d,l} \right] . \end{aligned} \tag{16}$$

Here Υ_n, $L_{d,l}$, and $I_{d,l}$ are defined by

$$\Upsilon_n(\psi) \equiv \frac{3}{4} \frac{(\int_o^{\lambda_c} d\lambda \ \Lambda_n)^2}{-\int_o^{\lambda_c} d\lambda \ (\frac{\partial}{\partial \lambda} < \xi >) \Lambda_n^2}, \tag{17}$$

$$L_{d,l}(\chi_o) \equiv \frac{1}{3\chi_o^{2d+2}} \int_o^{\chi_o} dt \frac{t^{2d+1}}{(1+t^3)^{l-1}} , \tag{18}$$

and

$$I_{d,l}(\chi_o, w_n) \equiv \frac{1}{3\chi_o^{2d+2}} \int_o^{\chi_o} \frac{dt}{(1+t^3)^l} \int_o^t dy \left\{ \left[\frac{y^3(1+t^3)}{t^3(1+y^3)} \right]^{w_n} \frac{d}{dy} \left[y^{2d+1}(1+y^3) \right] \right\} , \tag{19}$$

where, $\chi_o \equiv \frac{v_o}{v_c}$, $Q_p \equiv \frac{v_b^3}{v_c^3}$, $w_n \equiv \frac{Q_p \kappa_n}{3}$. It is noticed that the series for $C_{d,l}$ in Eq. (16) converges rapidly with respect to n; therefore the first few eigenfunctions and eigenvalues will suffice to provide quite accurate results for the radial fluxes Γ_{Neo}^d. This can be understood from (i) the fact that $\kappa_n > 2n^2 - n$ as will be shown in the next section (also c.f. Ref. [5]), and (ii) from the limiting form of Eq. (19)

$$I_{d,l} \simeq \frac{1}{w_n} \left\{ \frac{2d+4}{3} L_{d,l-1}(\chi_o) - L_{d,l}(\chi_o) \right\} + O\left(\frac{1}{w_n^2} \right)$$

deduced from partial integration and assuming $w_n \to \infty$.

It is important to note that χ_o characterizes the electron drag effect (i.e. for larger χ_o, electron drag dominates for a longer period during the slowing-down process), and Q_p marks the pitch angle scattering effect. However, whether the dominating effects are due to pitch angle scattering or drag is not at all a trivial question, since $C_{d,l}$ involves three independent parameters, χ_o, Q_p and ϵ. Detailed discussions of the results will be given in Secs. (III) and (IV). Here, in particular, we point out that while $Q_p = 0$ is a singular limit, for smaller but finite Q_p, it requires larger κ_n to make $I_{d,l} \propto \frac{1}{\kappa_n}$, i.e., the convergence needed to provide an accurate approximation to $C_{d,l}$ is delayed. This also implies that for smaller Q_p, more eigensolutions with respect to n are required to retain the correct dynamics near the trapped-passing boundary and to accurately approximate the exact solution. On the other hand, in practice, Q_p, which corresponds to some sort of mass ratio of the fast ions to the background ions, is usually of order unity.

III. Solutions and Results

In this section, we will numerically solve for the first few eigensolutions for various values of ϵ. For instructive purposes, we also derive analytically the eigensolutions using the Legendre expansion and the perturbation theory, assuming very small ϵ. The results from the perturbation analysis are then used for discussing several interesting limiting cases and limiting results from previous calculations. Moreover, the comparisons between the numerical results and the analytic approximations will be given.

A. Numerical Solutions

By assuming a concentric circular flux geometry (where the Jacobian $J = h = 1 + \epsilon cos\theta$), the eigenequation Eqs. (10) will be solved rigorously for finite ϵ. That is, the functionals $< \xi >$ and $\frac{\partial <\xi>}{\partial \lambda} = -\frac{1}{2} < \frac{1}{h\xi} >$ are numerically calculated to retain the complete finite ϵ effects. Then, by utilizing the asymptotic behaviors near the boundaries, Eqs. (10c), and adopting the IMSL routine BVPMS, we obtain the exact eigenfunctions Λ_n, eigenvalues κ_n, and Υ_n for $n = 1$ to 5 and $\epsilon = 0.01, 0.04, 0.09, \frac{1}{6}, \frac{1}{3}$, and $\frac{1}{2}$ (see Figs. (1)). The orthogonality of Λ_n and the variational form of eigenvalues κ_n given in Eq. (11) has been checked to ensure an accuracy such that the error is found $\leq 10^{-4}$.

It is interesting to note that the lowest eigenfunction is found to satisfy $\Lambda_1 = \Lambda_{pa} + 0(\sqrt{\epsilon})$ (see Fig. (2)), where

$$\Lambda_{pa} = \int_{\lambda}^{\lambda_c} \frac{d\lambda}{<\xi>} \Big/ \int_{0}^{\lambda_c} \frac{d\lambda}{<\xi>} \tag{20a}$$

is deduced from Eqs. (10b) and $\frac{\partial \Lambda_{pa}}{\partial \lambda} \propto \frac{1}{<\xi>}$. Hence, the lowest eigenvalue κ_1, for small ϵ, can be approximated by inserting Λ_{pa} into the variational form Eq. (11). This yields,

$$\kappa_1 = 1 + 1.47\sqrt{\epsilon} + 0(\epsilon). \tag{20b}$$

On the other hand, since the form for Υ_n in Eq. (17) is not variational, one can only approximate Υ_1 from Λ_{pa} to 0(1), i.e., $\Upsilon_1 \simeq 1$.

From the exact eigensolutions obtained here, the radial fluxes, or the normalized transport coefficients $C_{d,l}$ defined in Eq. (16), can be readily determined for given χ_o, Q_p and ϵ. In Figs. (3), we present $C_{d,1}$ *vs.* $\sqrt{\epsilon}$ for various realistic parameters. In particular, in Fig. (3a), (3b), we present $C_{d,1}$ for $Q_p = \frac{3}{5}$ and $\chi_o = 0.5, 1, 3, 6$. Also, $C_{d,1}$ for fast alphas in D-T and D-He^3 reactions and fast protons in D-He^3 reaction are presented in Figs. (3c), (3d). For the D-T reaction, we take the temperature to be 10KeV, and in D-He^3 reaction, we take the temperature to be 100KeV. Note that in both figures, the previously evaluated results given in Refs. [1] and [4] are also presented for comparison. It is shown that, except for the cases of larger $\epsilon(\sim 0.5)$ and small χ_o (for which pitch angle scattering is important even for finite magnetic well depth), the exact results are in between of the previously obtained limited results for most of the realistic parameter regimes. To understand these numerical results with more physical insight, it is useful to have an analytical approximation to the eigensolutions. We will therefore solve Eqs. (10) by using the perturbation theory in the next subsection.

B. Perturbation Theory For $\sqrt{\epsilon} \ll 1$

By defining a new variable $\eta \equiv \sqrt{1 - \frac{\lambda}{\lambda_c}}$, Eqs. (10) can be rewritten as

$$\frac{\partial}{\partial \eta}(1-\eta^2)\frac{<\xi>}{\eta}\frac{\partial}{\partial \eta}\Lambda_n = -2\kappa_n \frac{\partial <\xi>}{\partial \eta}\Lambda_n \tag{21a}$$

and

$$\begin{cases} \Lambda_n(\eta = 0) = 0, \\ \Lambda_n(\eta = 1) = 1. \end{cases} \tag{21b}$$

For $\epsilon = 0$, one finds that $\frac{<\xi>}{\eta} = \frac{\partial <\xi>}{\partial \eta} = 1$, and Eq. (21a) yields the eigensolutions

$$\begin{cases} \Lambda_n^{(0)} = P_{2n-1}(\eta), \\ \kappa_n^{(0)} = 2n^2 - n, \end{cases}$$

where the superscript (0) denotes $\epsilon = 0$ limit and P_{2n-1} is the usual Legendre polynomial. Hence, for nonzero ϵ, it should be useful to expand the full solution Λ_n in series of Legendre polynomial. A naive attempt fails to converge, however, because of the singularity of $\frac{\partial <\xi>}{\partial \lambda}$ near the trapped passing boundary.

In order to take into consideration the asymptotic behavior near the trapped-passing boundary, as in Eq. (10c), we set

$$\Lambda_n(\eta) = \frac{\eta}{<\xi>} \sum_{m=1}^{\infty} a_{nm} P_{2m-1}(\eta) \ , \tag{23}$$

Then, by using the properties of Legendre polynomial, $\left[\int_o^1 d\eta \ P_{2l-1}(\eta)\cdot\text{Eq. (21a)}\right]$ yields

$$\frac{\kappa_n - \kappa_l^{(0)}}{4l-1} a_{nl} = -(l-1/2)) \sum_{m=1}^{\infty} a_{nm} \int_o^1 d\eta \left[\frac{P_{2l-2}P_{2m-1}}{\eta}\left(1 - \frac{\eta}{<\xi>}\frac{\partial <\xi>}{\partial \eta}\right)\right]$$
$$+ (\kappa_n - l + 1/2) \sum_{m=1}^{\infty} a_{nm} \int_o^1 d\eta \left[P_{2l-1}P_{2m-1}\left(1 - \frac{\eta}{<\xi>}\frac{\partial <\xi>}{\partial \eta}\right)\right] \ , \tag{24}$$

Now by assuming $\sqrt{\epsilon} \ll 1$ in concentric circular flux geometry, it is found that

$$<\xi> = \frac{2}{\pi}\sqrt{\eta^2 + 2\epsilon}\ E\left(\frac{2(1+\eta^2)\epsilon}{\eta^2 + 2\epsilon}\right) + O(\epsilon)$$

which leads to, (see also Fig. (4)),

$$1 - \frac{\eta}{<\xi>}\frac{\partial <\xi>}{\partial \eta} \simeq \begin{cases} 1 & \text{for } \eta^2 \ll \epsilon \\ O(1) & \text{for } \eta^2 \sim O(\epsilon) \\ \epsilon/\eta^2 & \text{for } \eta^2 \gg \epsilon \end{cases}$$

where $E(x) \equiv \int_o^{\frac{\pi}{2}} d\theta (1 - x\sin^2\theta)^{1/2}$ is the complete elliptic integral of the second kind. Therefore

$$\Delta_\xi \equiv \int_o^1 d\eta \ \left(1 - \frac{\eta}{<\xi>}\frac{\partial <\xi>}{\partial \eta}\right) \simeq O(\sqrt{\epsilon})$$

and for $n \geq 1$

$$\int_o^1 d\eta \ \left(1 - \frac{\eta}{<\xi>}\frac{\partial <\xi>}{\partial \eta}\right)\eta^{2n} = O(\epsilon) \ .$$

The perturbation analysis is thus achieved by omitting $O(\epsilon)$ from Eq. (24) to yield

$$\tilde{\kappa}_n \equiv \kappa_n - \kappa_n^{(0)} \simeq \frac{4n-1}{3}\left(\frac{(2n-1)!!}{(2n-2)!!}\right)^2 \tilde{\kappa}_1 \tag{25}$$

$$\tilde{a}_{nm} \equiv a_{nm} - \delta_{nm} \simeq \frac{4m-1}{3}\left[\frac{(2m-1)!!}{(2m-2)!!}\frac{(2n-1)!!}{(2n-2)!!}\right](-1)^{n+m}\frac{\tilde{\kappa}_1}{\kappa_n^{(0)} - \kappa_m^{(0)}} \tag{26a}$$

$$\tilde{a}_{nn} \equiv a_{nn} - 1 = \sum_{m \neq n} a_{nm} \ , \tag{26b}$$

where $\tilde{\kappa}_1 = \kappa_1 - 1$ is according to Eq. (20b). Furthermore, from Eqs. (23), (25) and (26), Eq. (17) yields

$$\Upsilon_n \simeq \frac{4n-1}{3} (\tilde{a}_{n1})^2 \sim O(\epsilon) \tag{27a}$$

and

$$\Upsilon_1 = (1-\epsilon)^2 \left\{ 1 + 6 \int_o^1 d\eta \, \eta^2 \left(1 - \frac{\eta}{<\xi>} \right) \right\} - \sum_{n=2}^{\infty} \Upsilon_n + O(\epsilon^{3/2}) \ .$$

Here by using the facts that $\frac{\partial}{\partial \epsilon} < \xi > \Big|_{\epsilon=0} = \frac{1-\eta^2}{2\eta}$ and $< \xi > \Big|_{\epsilon=0} = \eta$, one finds $\int_o^1 d\eta \, \eta^2 \left(1 - \frac{\eta}{<\xi>} \right) \simeq 2\epsilon$; hence,

$$\Upsilon_1 = 1 - \sum_{n=2}^{\infty} \Upsilon_n + O(\epsilon^{3/2}) \ . \tag{27b}$$

Now we are able to make comparisons of numerical results with the analytic predictions based upon the perturbation analysis given above. First, we numerically fit the numerical solution Λ_n obtained in subsection (III.A) with the modified Legendre polynomial expansion in the form

$$\Lambda_n = \frac{\eta}{<\xi>} \sum_{m=1}^{8} a_{nm}(\epsilon) P_{2m-1}(\eta) \ . \tag{28}$$

Then, the coefficients $\tilde{a}_{nm}(\epsilon) \equiv a_{nm}(\epsilon) - \delta_{nm}$ are fitted with the polynomial form

$$\tilde{a}_{nm}(\epsilon) = \sum_{k=1}^{4} \alpha_{nm}^{(k)} \epsilon^{k/2}$$

The coefficients $\alpha_{nm}^{(k)}$ are given in Table I, and it is found that the coefficients $\alpha_{nm}^{(1)}$ are in good agreement with the analytic prediction given by Eqs. (26), within 10%.

For transport fluxes, the normalized transport coefficients $C_{d,l}$ for $Q_p = \frac{3}{5}$ and $\chi_o = 0.5, 3.0$, numerically obtained in Sec III.A, are fitted in powers of $\sqrt{\epsilon}$ such that

$$C_{d,l} = \sum_{k=1}^{4} \beta_{d,l}^{(k)} \epsilon^{k/2} \ .$$

The coefficients $\beta_{d,l}^{(k)}$ are given in Table II; and again, good agreement is found between $\beta_{d,l}^{(1)}$ and the analytic prediction given in Eq. (29a) in the next subsection, with error bounds of 10%. On the other hand, for the case of $\chi_o = 3.0$, the large value of the coefficients $\beta_{d,l}^{(3)}$ implies that small ϵ approximation is no longer valid for the parameters $\chi_o = 3.0$ and $Q_p = \frac{3}{5}$. From the discussions following Eq. (30b) in the next subsection, it will become clear that this $\epsilon^{3/2}$ scaling is due to the domination of the drag effects.

Moreover, with the perturbation analysis given in this subsection, one is able to further study the limiting forms of $C_{d,l}$ from Eq. (16) to obtain better physics insight. This is given in the next subsection.

Table I. Polynomial Fit for Eigenfunctions

$$\tilde{a}_{nm} \equiv a_{nm} - \delta_{nm} = \sum_{k=1}^{4} \alpha_{nm}^{(k)} \epsilon^{k/2}$$

$$\alpha_{nm}^{(k)}$$

$(n,m) \backslash k$	1	2	3	4
$(1,1)$	-0.62	1.33	-2.30	3.08
$(2,1)$	-0.45	-0.13	1.03	-2.04
$(1,2)$	1.00	-3.26	7.32	-11.14
$(2,2)$	-0.59	1.93	-4.95	8.32
$(2,3)$	1.62	-4.74	11.55	-18.87
$(3,2)$	-1.10	0.34	1.70	-4.60
$(3,3)$	-0.56	0.85	-3.46	7.34
$(3,4)$	2.22	-5.32	11.83	-1.92
$(4,3)$	0.54	0.49	-2.22	4.21
$(4,3)$	-1.76	1.93	-0.23	-2.85
$(4,4)$	-5.36	-1.55	2.08	-0.19
$(4,5)$	2.85	-5.61	9.70	-15.00
$(5,3)$	0.89	0.31	-2.61	4.74
$(5,4)$	-2.41	4.35	-3.66	0.68
$(5,5)$	-0.56	-4.62	9.51	-9.06
$(5,6)$	3.43	-4.92	1.50	1.78

Table II. Polynomial Fit for The Normalized Transport Coefficients

$$C_{d,l} = \sum_{k=1}^{4} \beta_{d,l}^{(k)} \epsilon^{k/2}$$

$$\beta_{d,l}^{(k)} \times 10^2$$

$$\frac{v_o}{v_c} \equiv \chi_o = 0.5$$

$(d,l) \backslash k$	1	2	3	4
$(0,1)$	14	23	12	18
$(0,2)$	13	22	11	17
$(1,1)$	7	20	30	20
$(1,2)$	6.5	19	28	19

$$\frac{v_o}{v_c} \equiv \chi_o = 3.0$$

$(d,l) \backslash k$	1	2	3	4
$(0,1)$	2.85	8.85	18.5	17.3
$(0,2)$	1.3	2.74	3.24	3.28
$(1,1)$	0.61	7.64	29	27
$(1,2)$	0.12	0.86	2.68	2.37

C. Limiting Results And Comparisons With Previous Calculations

Let us first study the pitch angle scattering dominant case, i.e., assuming large Q_p but finite ϵ and χ_o. By using the fact, for $Q_p \gg 1$, that $I_{d,l} \propto \frac{1}{Q_p}$, Eq. (16) yields

$$C_{d,l} \simeq Q_p \left[< h^2 > - \sum_{n=1}^{\infty} \frac{\Upsilon_n}{\kappa_n} \right] L_{d,l+1}(\chi_o) \tag{29a}$$

We should nevertheless note that Q_p is basically an ion mass ratio (see Eq. (2)); therefore, it will be unrealistic to assume Q_p to be very large. However, there is another parameter which can also obviously make pitch angle scattering dominant, i.e., the aspect ratio. We therefore assume very small ϵ but finite Q_p and χ_o from Eq. (16) which yields

$$C_{d,l} \simeq 1.47 Q_p \sqrt{\epsilon} L_{d,l+1}(\chi_o) \tag{29b}$$

with the validity condition

$$\epsilon \ll Q_p \frac{L_{d,l+1}(\chi_o)}{L_{d,l}(\chi_o)} \tag{29c}$$

The drag dominant limit can be achieved by assuming very large χ_o but finite ϵ and Q_p. From Eqs. (18) and (19), we have, for $\chi_o \gg 1$,

$$I_{d,1} \simeq L_{d,1} \gg I_{d,2}, L_{d,2}, L_{d,3}; \tag{30a}$$

Eq. (16) thus yields

$$C_{d,1} \simeq (2d+1) \left(< h^2 > - \sum_{n=1}^{\infty} \Upsilon_n \right) L_{d,l}(\chi_o) \tag{30b}$$

$$C_{d,2} \ll C_{d,1} \tag{30c}$$

We note here that it should be very careful when one further takes the small ϵ limit of Eq. (30b), since no matter how large χ_o is, there always exists a small enough quantity of ϵ that can make the pitch angle scattering effects important, as implied by Eq. (29b). This occurs when the magnetic well becomes so shallow that a weak pitch angle scattering can detrap the trapped particles easily. On the other hand, it is still very interesting to

note that, from Eq. (27b), the leading order term of Eq. (30b), in inverse aspect ratio, is $O(\epsilon^{\frac{3}{2}})$. That is, for the parameter regime in which χ_o is large enough that the inequality in Eq. (30a) is satisfied, and ϵ is small enough that

$$\left(< h^2 > - \sum_{n=1}^{\infty} \Upsilon_n \right) \propto \epsilon^{3/2}$$

is a good approximation, but is large enough that the inequality

$$\epsilon \gg Q_p \frac{L_{d,l+1}(\chi_o)}{L_{d,l}(\chi_o)}$$

still holds, one can expect that $C_{d,1} \propto \epsilon^{3/2}$ which might explain the observation from a Fokker-Planck Monte-Carlo simulation. Since Eqs. (29b) and (30b) appear to have similar leading order ϵ dependence as those of the previous limiting calculations by Nocentini[1] and Catto[4], it is therefore interesting to make further comparisons.

First we use the limiting solution for P given by Eqs. (8) to calculate the transport coefficients $C_{d,l}[P]$. Eq. (15) thus yields

$$C_{d,l}^{drag}[P_d] = \left(Q_p L_{d,l+1}(\chi_o) + (2d+1) L_{d,l}(\chi_o) \right) \left[< h^2 > + \frac{3}{4} \int_o^{\lambda_c} d\lambda \left(\frac{\partial < \xi >}{\partial \lambda} \right)^{-1} \right] \tag{31a}$$

and

$$C_{d,l}^{pa}[P_{pa}] = \left(Q_p L_{d,l+1}(\chi_o) + (2d+1) L_{d,l}(\chi_o) \right) \left[< h^2 > - \frac{3}{4} \int_o^{\lambda_c} d\lambda \frac{\lambda}{< \xi >} \right] \tag{31b}$$

Nocentini's and Catto's results are then recovered by taking both the $\chi_o \gg 1$ and $\epsilon \ll 1$ limits of $C_{d,l}^{drag}$ and $C_{d,l}^{pa}$, respectively, to yield

$$C_{d,l}^{Noc} \simeq 1.6 \cdot \frac{2d+1}{6(d+1)} \epsilon^{\frac{3}{2}} \tag{32a}$$

and

$$C_{d,l}^{Catto} \simeq 1.47 \cdot \frac{2d+1}{6(d+1)} \epsilon^{\frac{1}{2}}. \tag{32b}$$

Since both P_d and P_{pa} correspond to singular limits, as has been pointed out in preceding sections, it is therefore expected that Eqs. (31) do not agree with Eq. (29b) and (30b).

Moreover, it is also inconsistent either to take the small ϵ limit from a drag dominant solution or to take the large χ_o limit from a pitch angle scattering dominant solution. This is because (i) a very shallow magnetic well can allow for significant pitch angle randomization near the trapped-passing boundary even though the drag is dominant for most of the phase space; and because (ii) larger χ_o, on the other hand, can cause more banana orbits to collapse before the trapped particles are pitch angle scattered out of the banana orbits. In Figs. (3), we present $C_{d,1}^{Noc}$ and $C_{d,1}^{Catto}$ together with the exact $C_{d,1}$ for various realistic parameters. It is found that $C_{d,1}^{Noc}$ is underestimating and $C_{d,1}^{Catto}$ is overestimating the exact result for most of the practical parameter regimes.

Note further that by taking the small χ_o, large Q_p and small ϵ limit, $C_{d,1}^{pa}$ reduces to the limiting form given in Eq. (29b). This coincidence can be understood from the fact that P_{pa} can become a good approximation to the real solution when the above mentioned limits are fulfilled. This is because (i) $P_{pa} = \Lambda_{pa}\sigma_n[\Lambda_{pa}]$ (*c.f.* Eqs. (12b) and (20)); (ii) the singular limit, $Q_p \to \infty$, of Eq. (12a) yields a solution which coincides with its regular solution if $\kappa_n = 1$; (iii) for $\epsilon \ll 1$, we have found $\kappa_1 \simeq 1$ and $\Lambda_1 \simeq \Lambda_{pa}$ as pointed out in Eqs. (20); (iv) smaller value of χ_o reduces the term in Eq. (13) involving the velocity integral.

IV. Summary And Discussion

The general form of neoclassical transport fluxes of the fast ions generated from an isotropic source, in an axisymmetric plasma system, has been derived by a pitch angle scattering eigenfunction expansion, and is given by Eqs. (14)-(19). The fluxes can thus be readily determined upon solving the eigenequation Eqs. (10), with given Q_p, χ_o and ϵ. Therefore, the complete physics of pitch angle scattering, drag and finite aspect-ratio effects can be retained. Since the serial form of the transport coefficients $C_{d,l}$ in Eq. (16) shows rapid convergence, one needs only to solve for the first few eigensolutions.

It is concluded that either the pitch angle scattering-only solution or the drag-only solution is irrelevant, since they are associated with singular limits and violate the boundary condition either at the birth energy or at the trapped-passing boundary, i.e., at $v = v_o$ or at $\lambda = \lambda_c$. We would like to remark here that, from the above discussions, an immediate extension of the present work will be to evaluate the neoclassical transport of the plasma system with additional drag or energy diffusion terms which is usually thought to be negligible but in certain circumstances can play an important role[9]. Note that for typical parameter regimes, the radial losses are found to be in between those of previous evaluations[1,4] associated with the two limits.

The physical reality is that an energetic particle suffers mostly drag at birth; then, pitch angle scattering becomes more and more effective as the particle is slowed down by the drag. However, how fast it will enter the pitch angle scattering dominant region depends on its initial value of λ. A line roughly showing the boundary between the pitch angle scattering dominant region and the drag dominant region in the (v, λ) phase space is given in Fig. (5). In particular, in the trapped region, from Eqs. (5), (6), and the fact that P vanishes, the ratio of pitch angle scattering to drag is

$$\frac{C^{pa}(f_t)}{C^{drag}(f_t)} \sim \frac{v_b^3}{v^3 + v_c^3}; \tag{33a}$$

whereas, for barely passing particles,

$$\frac{C^{pa}(f)}{C^{drag}(f)} \sim \frac{v_b^3}{v^3 + v_c^3} \lambda \frac{\partial}{\partial \lambda} \left(\frac{\xi}{< \xi >} \right). \tag{33b}$$

Therefore, we are able to devide the phase space into three regions corresponding to the three classes of energetic particles as described in Sec. I.

If during a period τ_{eff}, a particle traverses a distance Δr due to some mechanism such as pitch angle scattering or drag induced banana collapse, the transport flux of such class of particles which suffers the same diffusion mechanism is roughly

$$\frac{\Delta r}{\tau_{eff}}\Big[n(r-\Delta r)-n(r+\Delta r)\Big].$$

Therefore, the diffusion coefficient of such a class of particles can be roughly estimated to be

$$D \sim F\,\frac{(\Delta r)^2}{\tau_{eff}},$$

where F is the fraction of such particles in phase space. Also, in the banana regime, where the bounce time τ_B of the trapped particle orbit is assumed to be much shorter than the slowing down time τ_s, one can qualitatively estimate the radial losses by only considering the contribution from the trapped particles for simplicity[10].

Then, by assuming $v_c \sim v_b \leq v_o$ and using Fig. (5), we estimate the diffusion coefficients as follows:

(i) for the pitch angle scattering dominant region I,

$$F \sim \frac{\sqrt{\epsilon}}{\chi_o}, \quad \Delta r \simeq \frac{\sqrt{\epsilon}\rho_p}{\chi_o} \qquad \text{and} \quad \tau_{eff} \sim \tau_s(\Delta\xi)^2 \sim \tau_s\Delta\lambda \sim \tau_s\epsilon,$$

i.e.,

$$D_1 \sim \frac{\sqrt{\epsilon}}{\chi_o^3}\frac{\rho_p^2}{\tau_s}; \tag{34a}$$

(ii) for the drag dominant region II, although there is negligible random pitch angle scattering, the particle will radially traverse a distance of $\Delta r \simeq \sqrt{\epsilon}\rho_p$ according to the shrinking of banana width during the slowing down process; in addition,

$$F \sim \sqrt{\epsilon} \quad \text{and} \quad \tau_{eff} \sim \tau_s,$$

therefore

$$D_2 \sim \frac{\rho_p^2}{\tau_s}\epsilon^{3/2}; \tag{34b}$$

(iii) for the intermediate region III, therefore $\frac{\Delta v}{v_c} \sim \Delta\xi$, so,

$$F \sim \frac{\Delta v}{v_o}\sqrt{\epsilon} \sim \frac{\epsilon}{\chi_o}, \quad \Delta r \simeq \frac{\sqrt{\epsilon}\rho_p}{\chi_o} \qquad \text{and} \quad \tau_{eff} \sim \tau_s \epsilon \ ,$$

i.e.,

$$D_3 \sim \frac{\rho_p^2}{\tau_s}\frac{\epsilon}{\chi_o^3}. \tag{34c}$$

To identify the physics origin of the transport fluxes from Eq. (16), we rewrite it in the following form

$$\begin{aligned} C_{d,l} = Q_p \left[< h^2 > - \sum_{n=1}^{\infty} \frac{\Upsilon_n}{\kappa_n} \right] L_{d,l+1} + (2d+1) \left[< h^2 > - \sum_{n=1}^{\infty} \Upsilon_n \right] L_{d,l} \\ + (2d+1) \sum_{n=1}^{\infty} \Upsilon_n \left(1 - \frac{1}{\kappa_n} \right)^2 (L_{d,l} - I_{d,l}) \ . \end{aligned} \tag{35}$$

Then, by following the discussions given in section III.B and C, we point out that, on the right hand side of Eq. (35), the first term ($\propto \epsilon^{\frac{1}{2}}$, for small ϵ) is due to the pitch angle scattering dominant region, the second term ($\propto \epsilon^{\frac{3}{2}}$, for small ϵ) is due to the drag dominant region, and the third term ($\propto \epsilon$, for small ϵ) is due to the region where both effects are of the same order.

To understand the practical significance of the radial losses of the energetic ions, two important time scales are introduced: (i) the time scale for the fast ions to slow down from birth to becoming Maxwellian "ash"

$$\hat{\tau}_d \equiv \frac{\int d\vec{v} \, (\frac{1}{2}mv^2)^d f(\vec{v})}{(\frac{1}{2}mv_o^2)^d S} \qquad d = 0, 1$$

(ii) the time scale for the radial losses

$$\tau_d \equiv \frac{\int d\vec{v} \, (\frac{1}{2}mv^2)^d f(\vec{v})}{\frac{1}{V'}\frac{\partial}{\partial\psi} V' \Gamma^d} \qquad d = 0, 1$$

The ratio of the two time scales thus becomes

$$\frac{\hat{\tau}_d}{\tau_d} \sim C_{d,l}\delta_p^2,$$

which measures the efficiency of transferring energy from the energetic ions to the background plasma. Since it is found in this work that $C_{d,l}$ is usually smaller than unity, the radial losses of the energetic ions will not become overly important as long as δ_p is sufficiently small.

However, we would like to note here that in modern devices, such as TFTR, JET and CIT, the fast ions produced from fusion reactions can have δ_p of order unity. In this case, our calculations are not reliable, since, as pointed out in Sec. II, our ordering scheme is based fundamentally upon the smallness of δ_p. Note that the immediate consequence of $\delta_p \sim 1$ is that the radial width of the trapped particle orbit becomes comparable to the radial scale length. This "fat banana" orbit effect to the energetic alphas transport near the magnetic axis was studied in Ref. [7] using only the drag portion of the collision operator, similar to Ref. [1] which assumed zero banana width. Since, for the thin banana case, the present work shows significant pitch angle scatttering driven enhancement over Ref. [1], it will be highly interesting to study the radial transport of fast ions by taking into account the fat banana effects and still retaining the complete physics of the drag, the pitch angle scattering, and the finite ϵ effects. We remark that to retain the complete physics in such a four dimensional system, the eigenfunction technique developed here should still be applicable for making the governing equation tractable. However, the bounce average would be performed along the exact large banana drift orbit extending across flux surface.

Acknowledgments

One of us (C. T. Hsu) is grateful to Prof. Jeffrey Freidberg for helpful discussions.

References

[1] A. Nocentini, M. Tessarotto, and F. Engelmann, Nucl. Fusion **15**, 359 (1975).

[2] P. J. Catto, Phys. Fluids **30**, 2740 (1987). The right side of Eqs. (28) and (33) should be divided by two.

[3] P. J. Catto and M. Tessarotto, Phys. Fluids **31**, 2292 (1988).

[4] P. J. Catto, Phys. Rev. Letters **60**, 1954 (1988).

[5] J. G. Cordey, Nucl. Fusion **16**, 499 (1987).

[6] For instance, T.H. Stix, Phys. Fluids **16**, 1922 (1973).

[7] V. Ya. Goloborod'ko, Ya. I. Kolesnichenko, and V. A. Yavorskij, Nucl. Fusion **23**, 399 (1983).

[8] M. N. Rosenbluth, R. D. Hazeltine, and F. L. Hinton, Phys. Fluids **15**, 116 (1972).

[9] A. A. Ware, Nucl. Fusion **25**, 185 (1985).

[10] F.L. Hinton and R.D. Hazeltine, Rev. Mod. Phys. **48**, 239 (1976).

Figure Captions

Figs. 1a-f Eigenfunctions Λ_n and eigenvalues κ_n of Eqs. (10), for $n = 1$ to 5 and $\epsilon = 0.01, 0.04, 0.09, \frac{1}{6}, \frac{1}{3}$, and $\frac{1}{2}$. Also, Υ_n defined in Eq. (17) are given. The Modified Legendre Polynomial Expansions are defined by Eq. (28).

Fig. 2 $\frac{\partial \Lambda_1}{\partial \Lambda_{pa}}$ for $\epsilon = 10^{-4}$, where Λ_{pa} is defined by Eq. (20a). This shows that $\Lambda_1 = \Lambda_{pa} + 0(\sqrt{\epsilon})$.

Figs. 3a,b The normalized particle diffusion coefficients $C_{0,1}$ and thermal diffusivity $C_{1,1}$, driven by $\frac{\partial}{\partial \psi} \ln(S\tau_s)$, *vs.* $\sqrt{\epsilon}$ for $Q_p = \frac{3}{5}$ and $\chi_o = 0.5, 1, 3, 6$. $C_{d,1}$ based on results from Nocentini[1] and Catto[4] are also shown for comparison. The coefficients $C_{d,l}$ are defined in Eq. (16).

Figs. 3c,d The normalized particle diffusion coefficients $C_{0,1}$ and thermal diffusivity $C_{1,1}$, driven by $\frac{\partial}{\partial \psi} \ln(S\tau_s)$, *vs.* $\sqrt{\epsilon}$ for fast alphas in D-T and D-He^3 reactions and fast protons in D-He^3 reaction.

Fig. 4 The functional $\left(1 - \frac{\eta}{<\xi>} \frac{\partial <\xi>}{\partial \eta}\right)$ given in Eq. (24) *vs.* variable $\eta \equiv \sqrt{1 - \frac{\lambda}{\lambda_c}}$ for $\epsilon = 10^{-4}$. It behaves qualitatively like a Gaussian with width $\sqrt{\epsilon}$.

Fig. 5 A line roughly showing where pitch angle scattering and drag forces are equal in the velocity space (v, λ) for barely passing particles and trapped particles, *cf.* Eqs. (33). The three regions in the trapped region are devided according to the discussions given in Secs. I and IV.

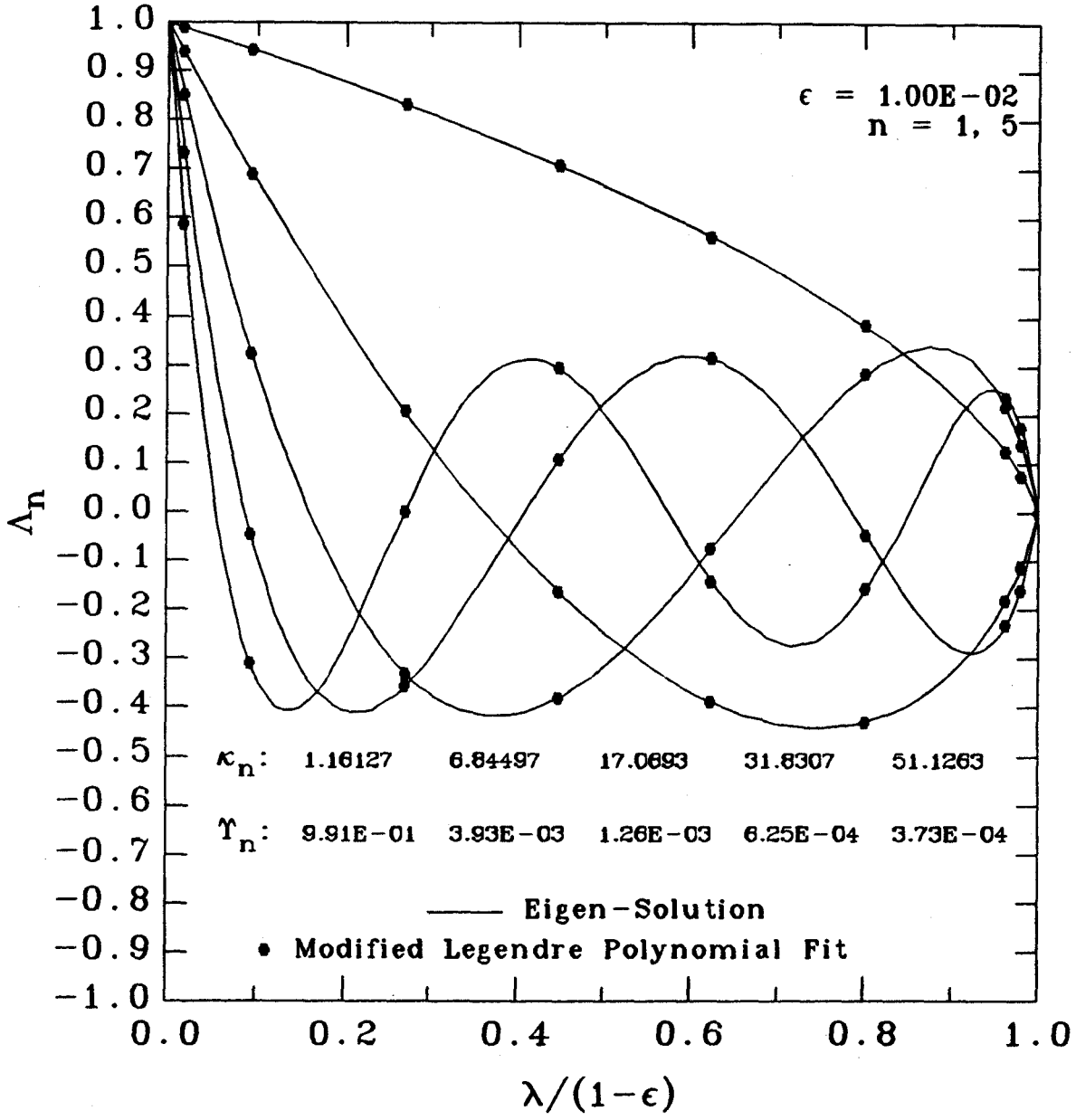
1.0
0.9
0.8
0.7
0.6
0.5
0.4
0.3
0.2
0.1
0.0
−0.1
−0.2
−0.3
−0.4
−0.5
−0.6
−0.7
−0.8
−0.9
−1.0
Λ_n
ϵ = 1.00E−02
n = 1, 5
κ_n: 1.16127 6.84497 17.0693 31.8307 51.1263
Υ_n: 9.91E−01 3.93E−03 1.26E−03 6.25E−04 3.73E−04
Eigen−Solution
Modified Legendre Polynomial Fit
0.0 0.2 0.4 0.6 0.8 1.0
$\lambda/(1-\epsilon)$

Fig. 1a

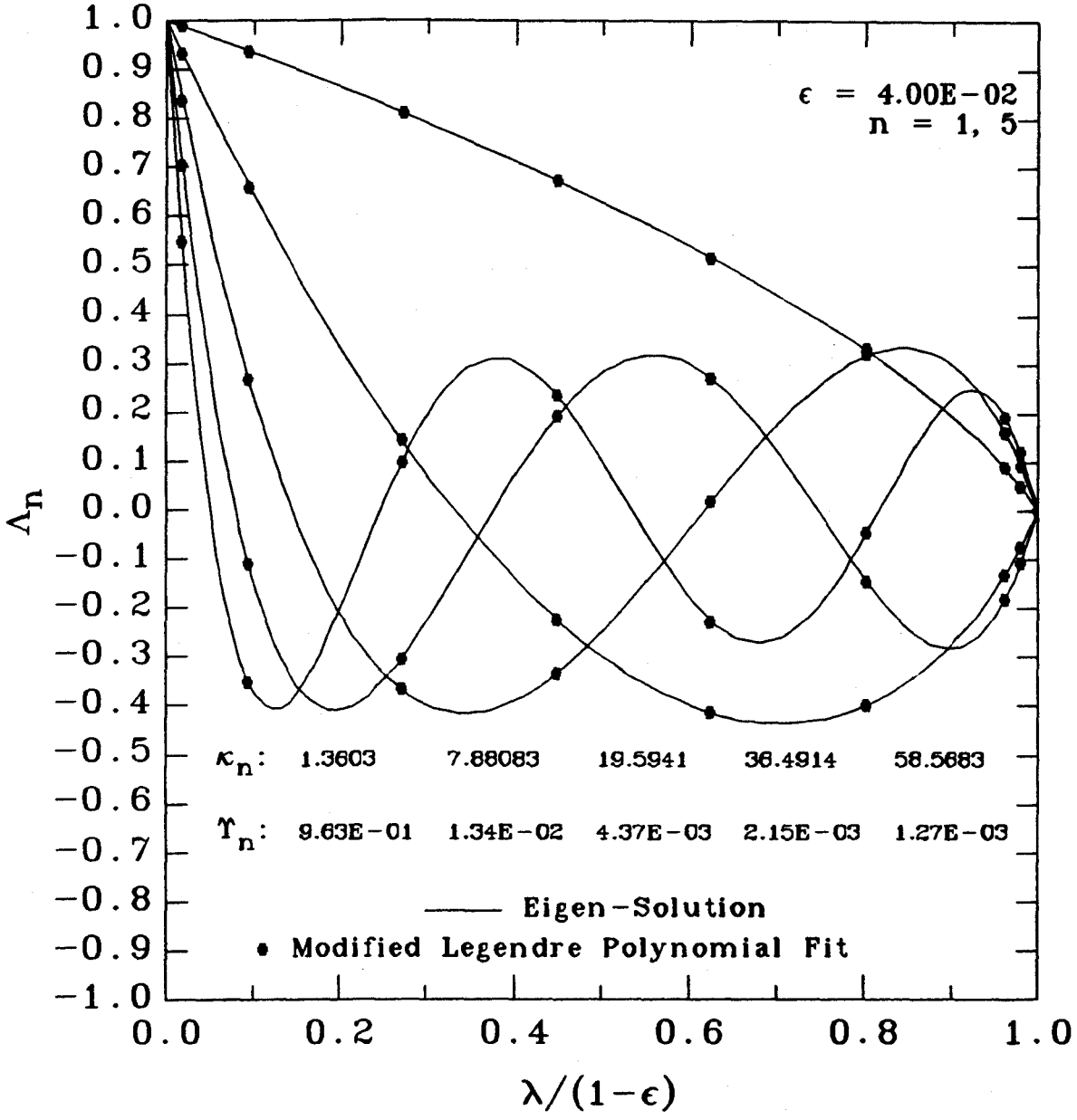
1.0
0.9
0.8
0.7
0.6
0.5
0.4
0.3
0.2
0.1
0.0
−0.1
−0.2
−0.3
−0.4
−0.5
−0.6
−0.7
−0.8
−0.9
−1.0
Λ_n
ϵ = 4.00E−02
n = 1, 5
κ_n: 1.3603 7.88083 19.5941 36.4914 58.5683
Υ_n: 9.63E−01 1.34E−02 4.37E−03 2.15E−03 1.27E−03
Eigen−Solution
Modified Legendre Polynomial Fit
0.0 0.2 0.4 0.6 0.8 1.0
$\lambda/(1-\epsilon)$

Fig. 1b

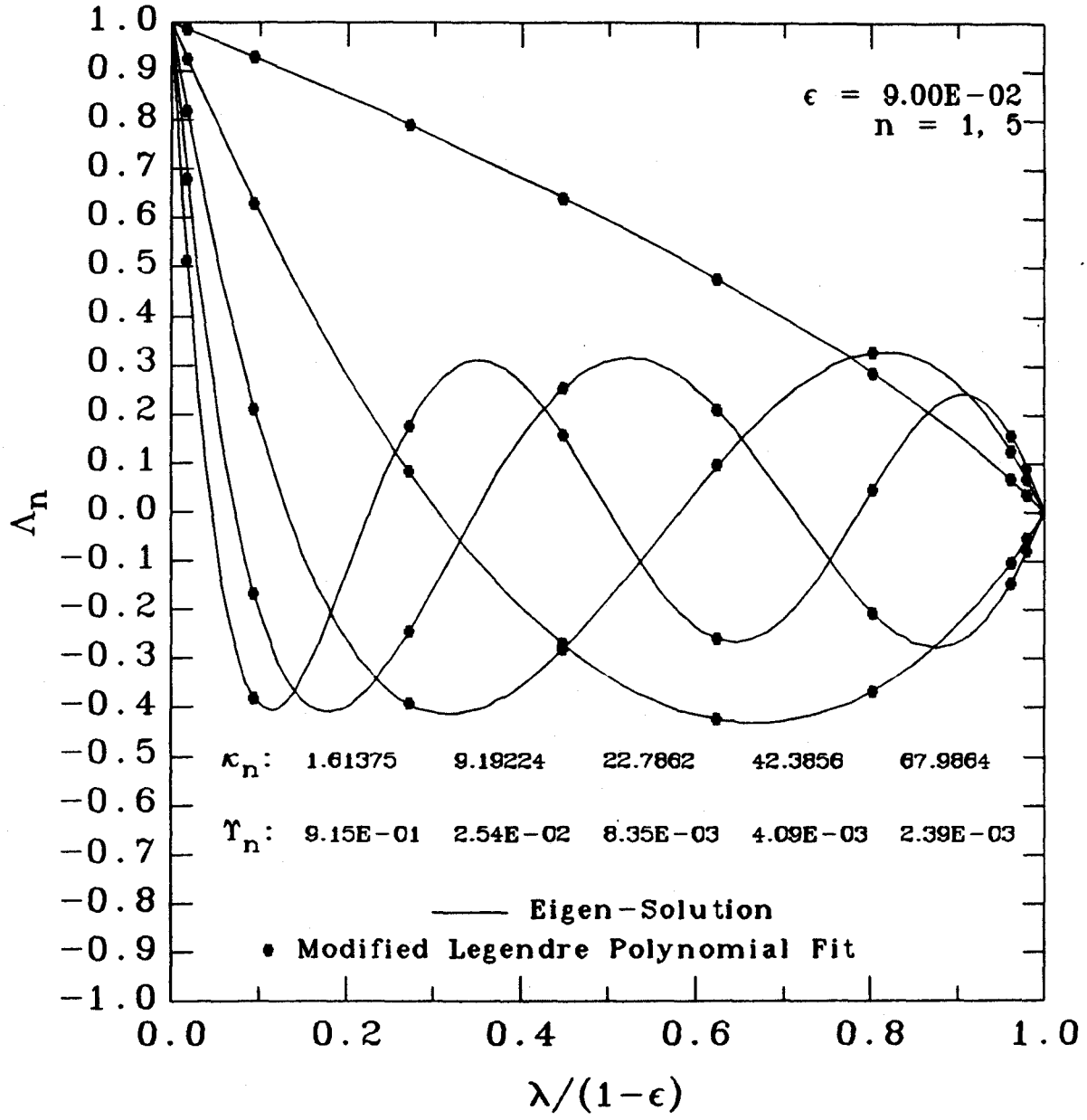
1.0
0.9
0.8
0.7
0.6
0.5
0.4
0.3
0.2
0.1
0.0
−0.1
−0.2
−0.3
−0.4
−0.5
−0.6
−0.7
−0.8
−0.9
−1.0
Λ_n
ϵ = 9.00E−02
n = 1, 5
κ_n: 1.61375 9.19224 22.7862 42.3856 67.9864
Υ_n: 9.15E−01 2.54E−02 8.35E−03 4.09E−03 2.39E−03
Eigen−Solution
Modified Legendre Polynomial Fit
0.0 0.2 0.4 0.6 0.8 1.0
$\lambda/(1-\epsilon)$

Fig. 1c

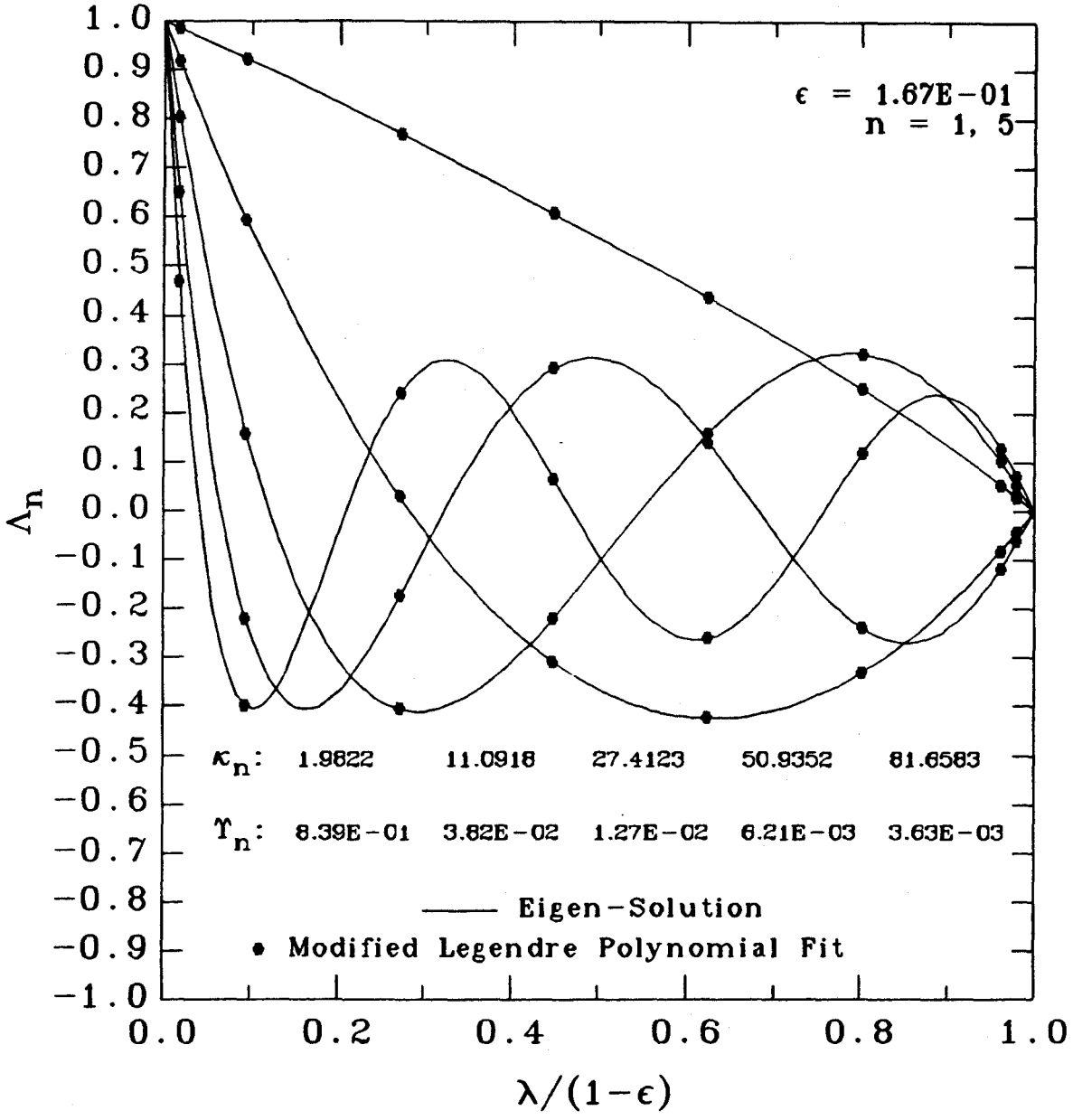
ϵ = 1.67E-01
n = 1, 5
κ_n: 1.9822 11.0918 27.4123 50.9352 81.6583
Υ_n: 8.39E-01 3.82E-02 1.27E-02 6.21E-03 3.63E-03
Eigen-Solution
Modified Legendre Polynomial Fit
Λ_n
$\lambda/(1-\epsilon)$
1.0
0.9
0.8
0.7
0.6
0.5
0.4
0.3
0.2
0.1
0.0
-0.1
-0.2
-0.3
-0.4
-0.5
-0.6
-0.7
-0.8
-0.9
-1.0
0.0
0.2
0.4
0.6
0.8
1.0

Fig. 1d

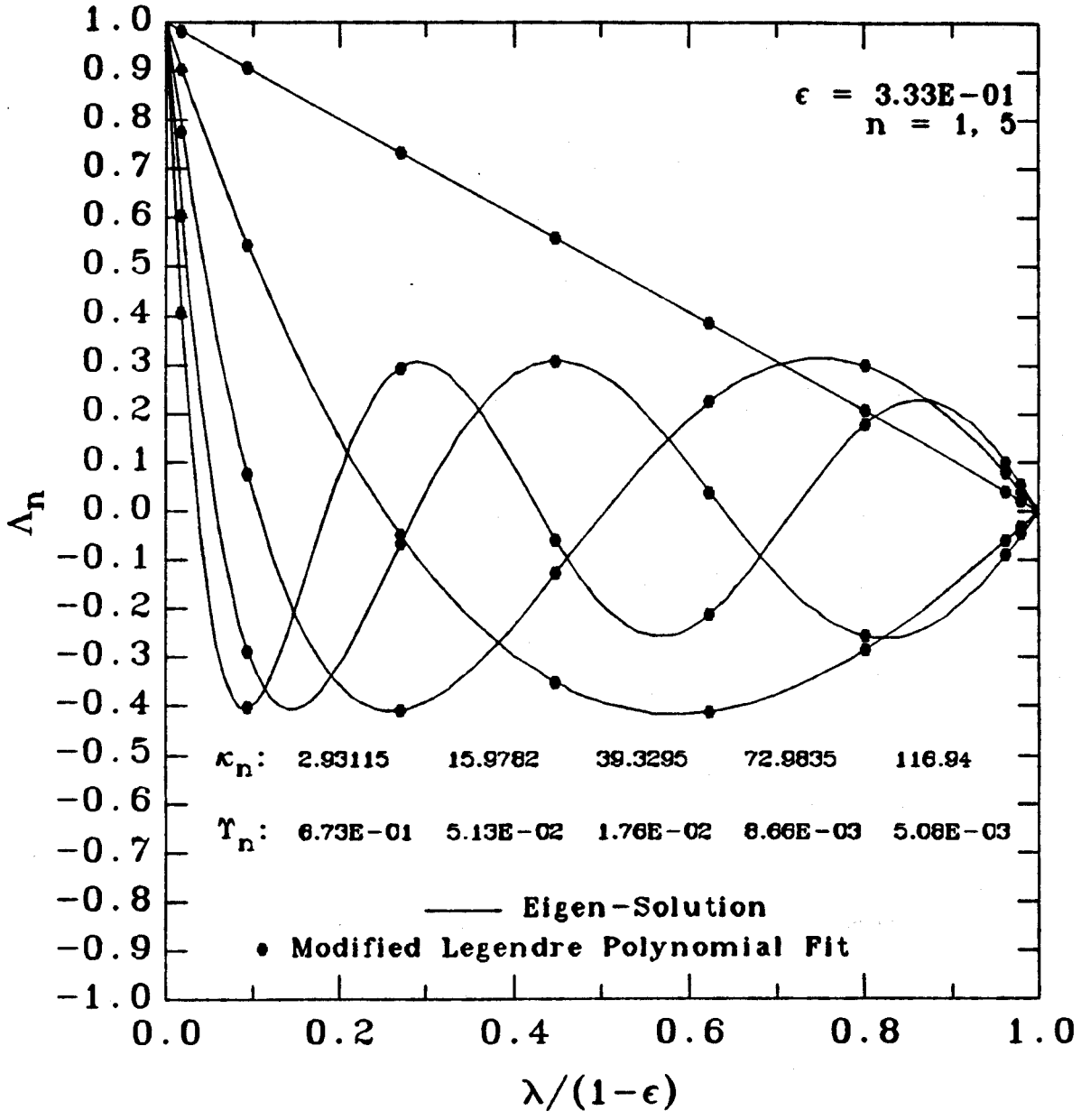
ε = 3.33E-01
n = 1, 5
Λ_n
κ_n: 2.93115 15.9782 39.3295 72.9835 116.94
Υ_n: 6.73E-01 5.13E-02 1.76E-02 8.66E-03 5.08E-03
Eigen-Solution
Modified Legendre Polynomial Fit
λ/(1-ε)

Fig. 1e

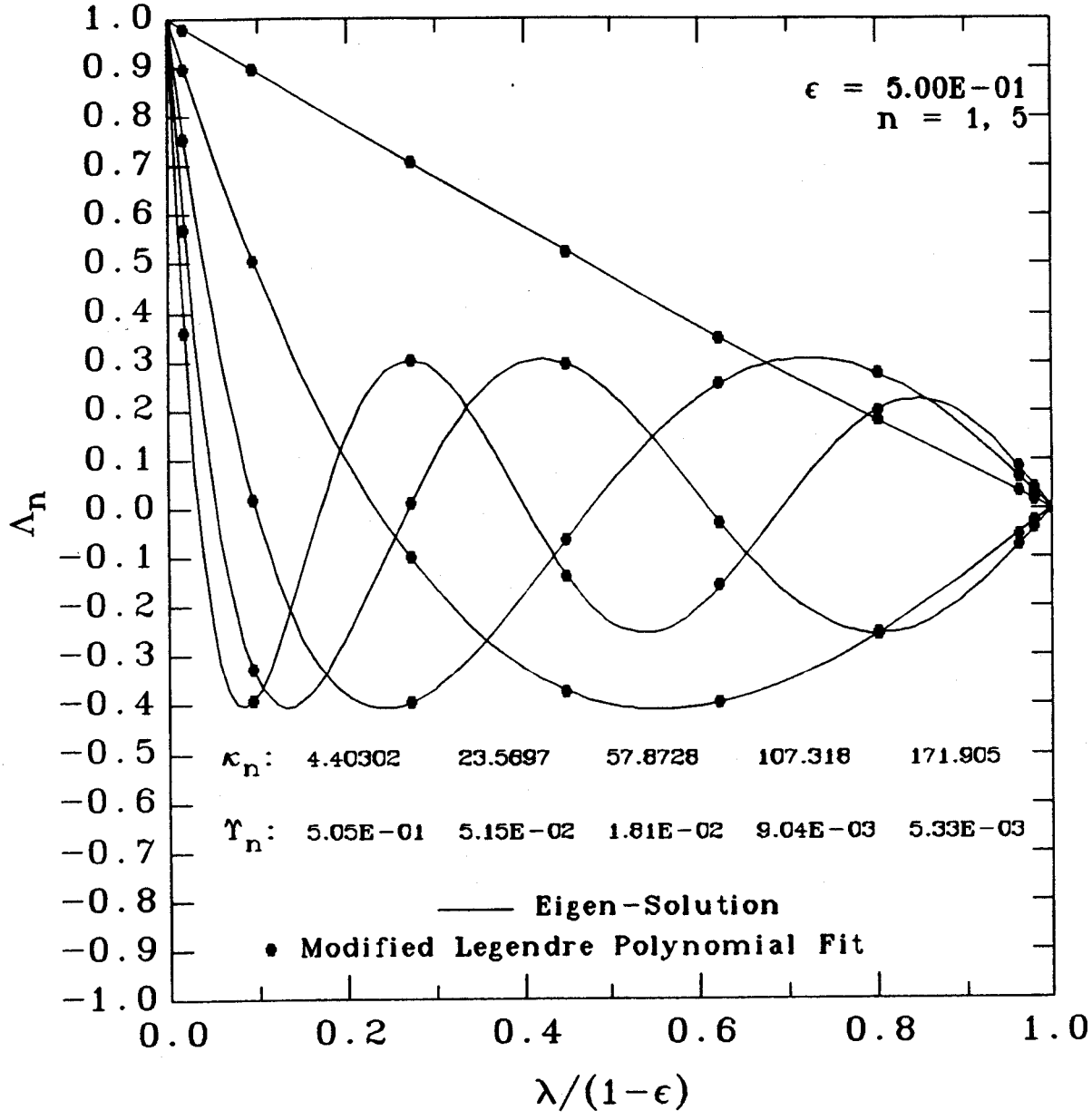
1.0
0.9
0.8
0.7
0.6
0.5
0.4
0.3
0.2
0.1
0.0
−0.1
−0.2
−0.3
−0.4
−0.5
−0.6
−0.7
−0.8
−0.9
−1.0
Λ_n
ϵ = 5.00E−01
n = 1, 5
κ_n: 4.40302 23.5697 57.8728 107.318 171.905
Υ_n: 5.05E−01 5.15E−02 1.81E−02 9.04E−03 5.33E−03
Eigen−Solution
Modified Legendre Polynomial Fit
0.0 0.2 0.4 0.6 0.8 1.0
$\lambda/(1-\epsilon)$

Fig. 1f

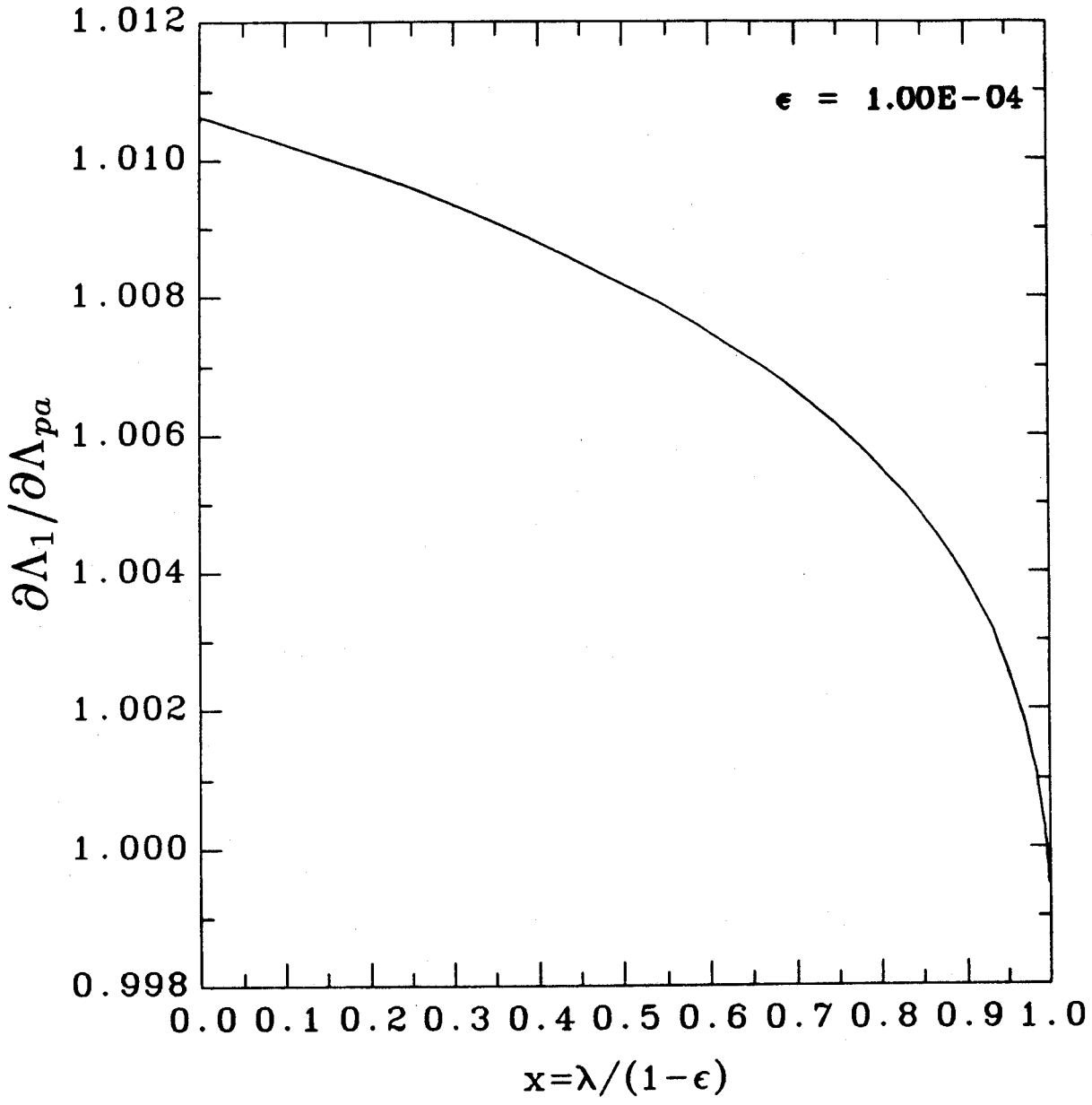
1.012
1.010
1.008
1.006
1.004
1.002
1.000
0.998
ϵ = 1.00E-04
$\partial\Lambda_1/\partial\Lambda_{pa}$
0.0 0.1 0.2 0.3 0.4 0.5 0.6 0.7 0.8 0.9 1.0
$x=\lambda/(1-\epsilon)$

Fig. 2

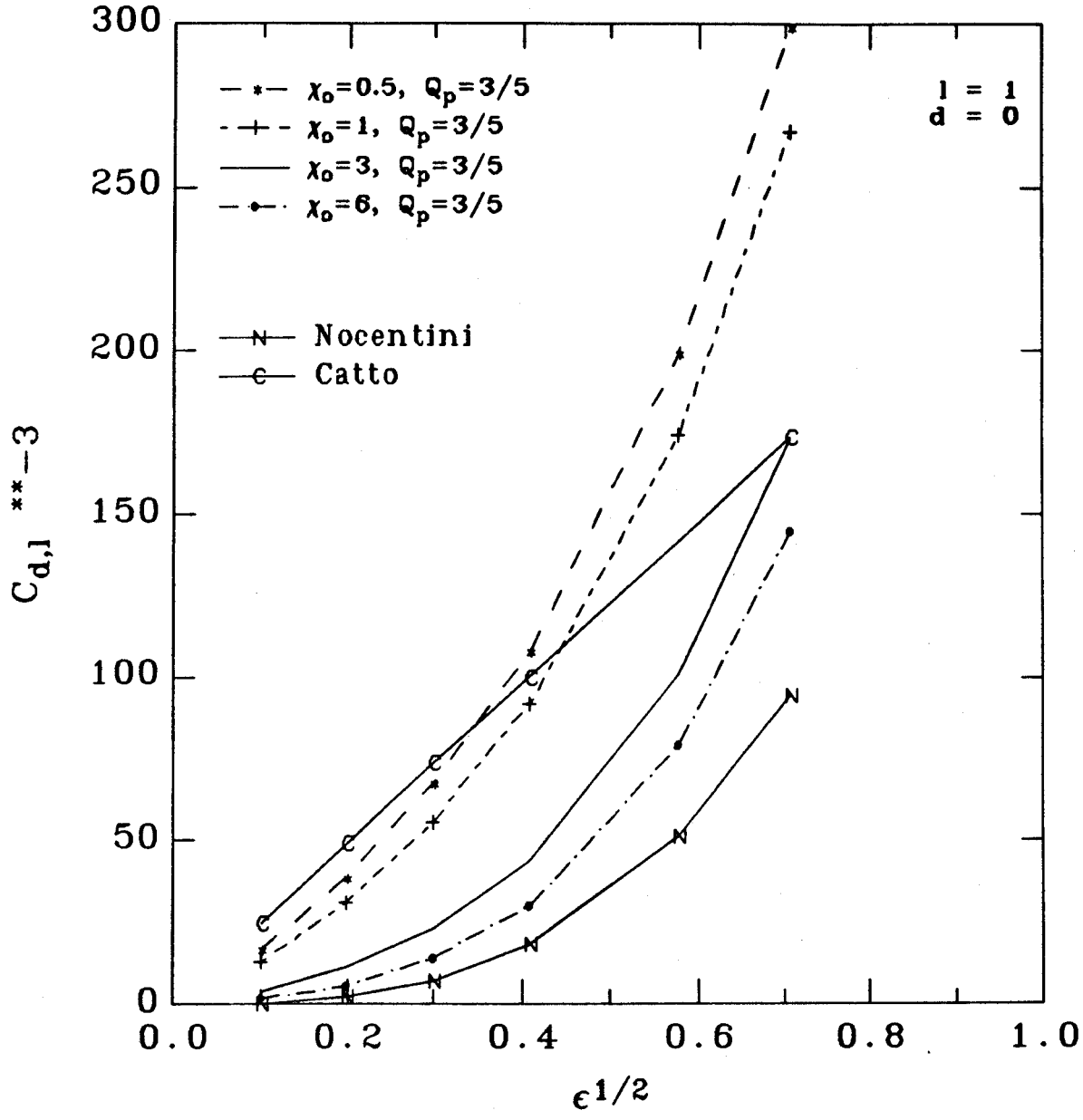
300
250
200
150
100
50
0
0.0
0.2
0.4
0.6
0.8
1.0
$\epsilon^{1/2}$
$C_{d,l}^{**}-3$
χ_o=0.5, Q_p=3/5
χ_o=1, Q_p=3/5
χ_o=3, Q_p=3/5
χ_o=6, Q_p=3/5
Nocentini
Catto
l = 1
d = 0

Fig. 3a

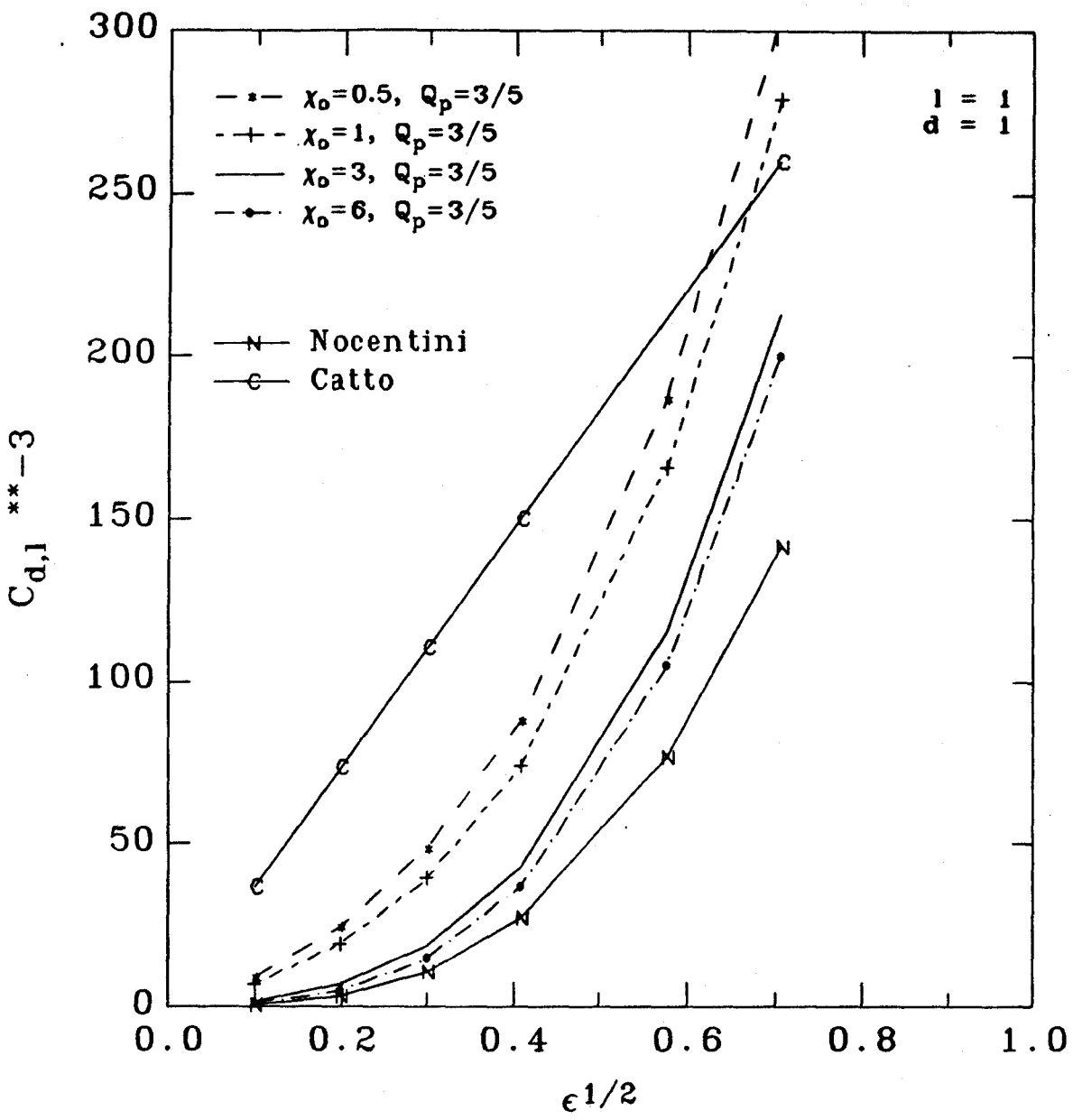
300
250
200
150
100
50
0
0.0
0.2
0.4
0.6
0.8
1.0
$C_{d,l}^{**-3}$
$\epsilon^{1/2}$
χ_o=0.5, Q_p=3/5
χ_o=1, Q_p=3/5
χ_o=3, Q_p=3/5
χ_o=6, Q_p=3/5
Nocentini
Catto
l = 1
d = 1

Fig. 3b

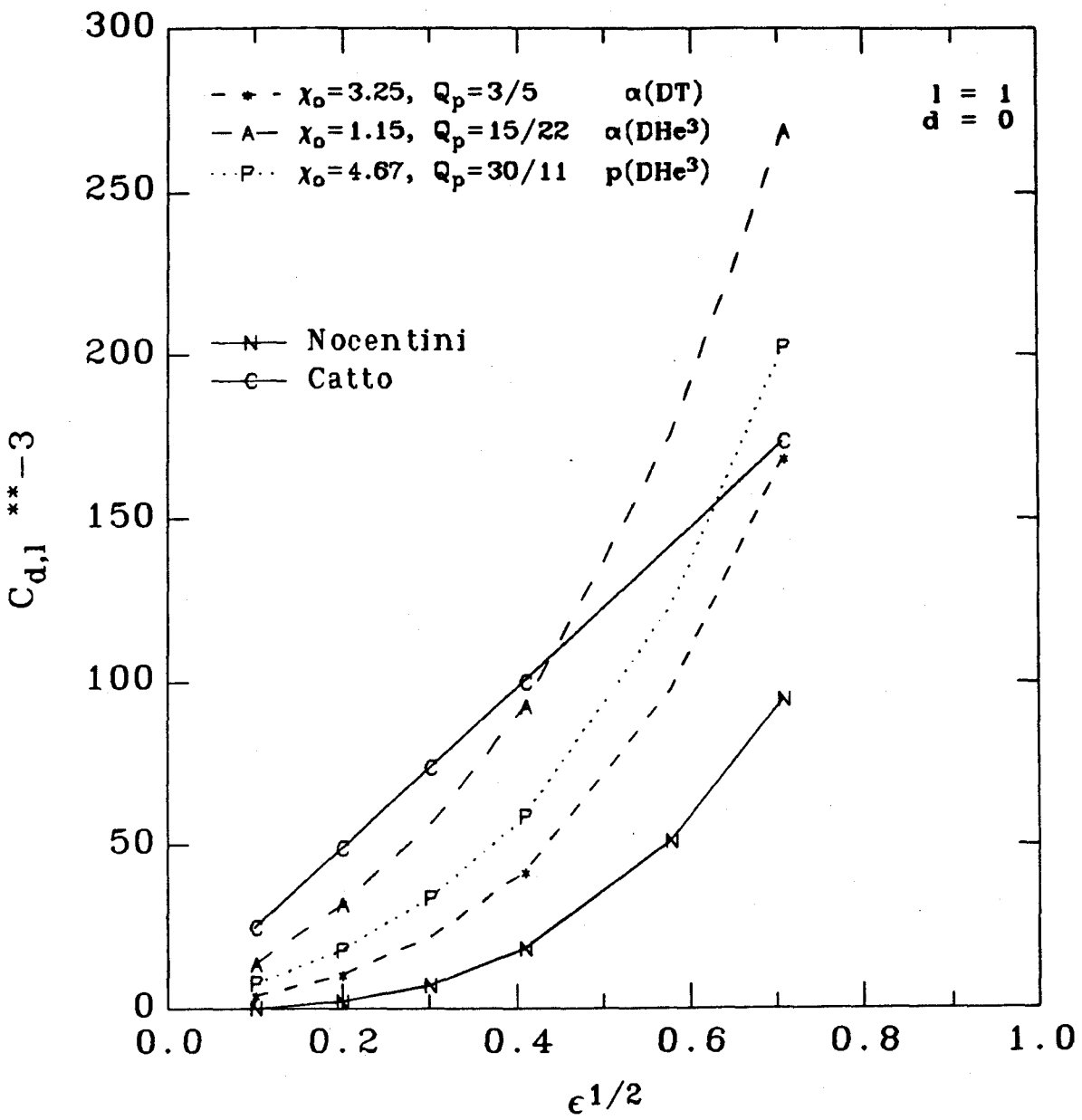
300
250
200
150
100
50
0
0.0
0.2
0.4
0.6
0.8
1.0
$C_{d,l}$ **-3
$\epsilon^{1/2}$
- * - χ_0=3.25, Q_p=3/5 α(DT)
— A— χ_0=1.15, Q_p=15/22 α(DHe³)
···P·· χ_0=4.67, Q_p=30/11 p(DHe³)
l = 1
d = 0
—N— Nocentini
—C— Catto

Fig. 3c

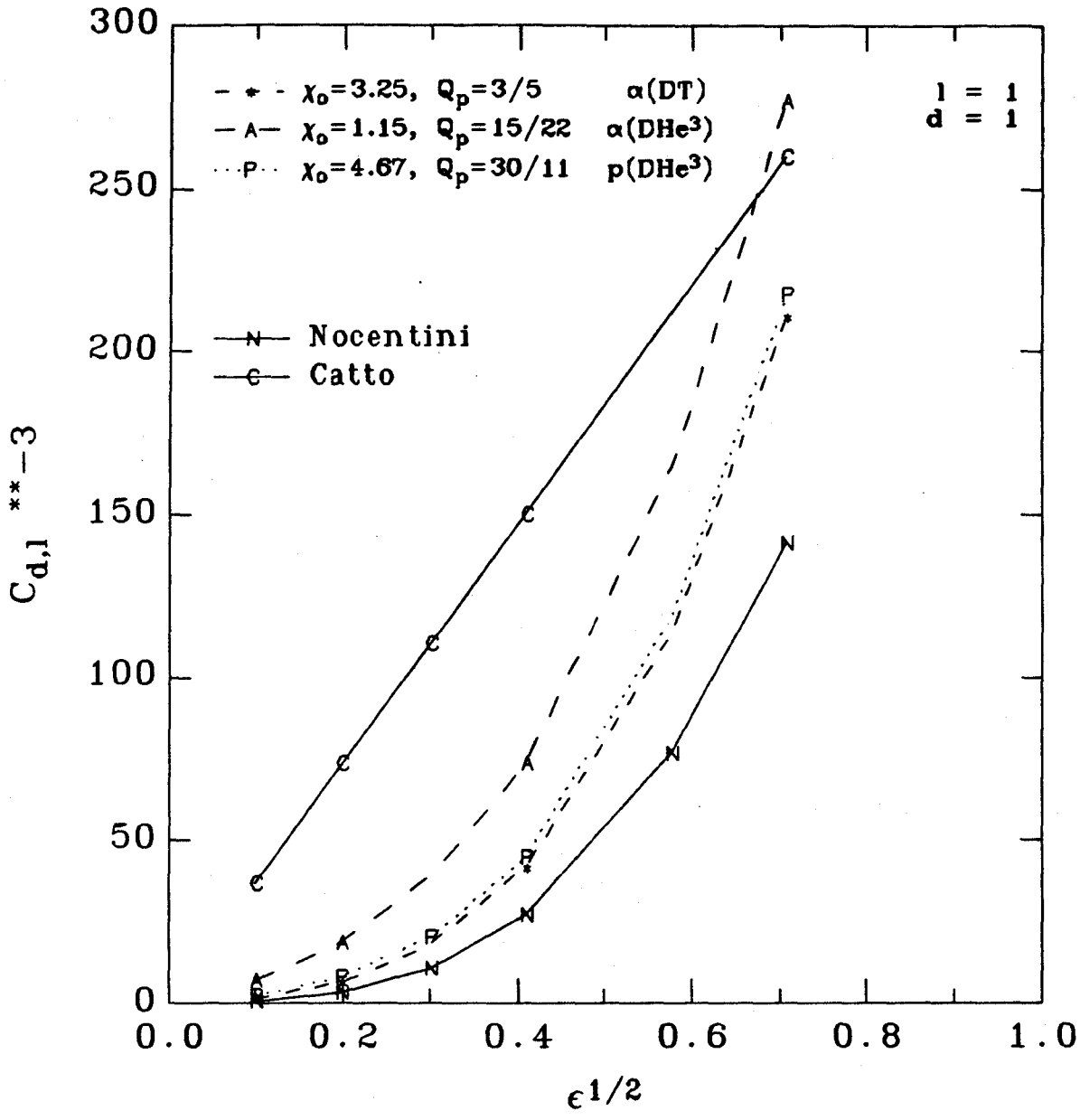
300
250
200
150
100
50
0
0.0
0.2
0.4
0.6
0.8
1.0
$C_{d,l}^{**-3}$
$\epsilon^{1/2}$
χ_0=3.25, Q_p=3/5 α(DT)
χ_0=1.15, Q_p=15/22 α(DHe³)
χ_0=4.67, Q_p=30/11 p(DHe³)
l = 1
d = 1
Nocentini
Catto

Fig. 3d

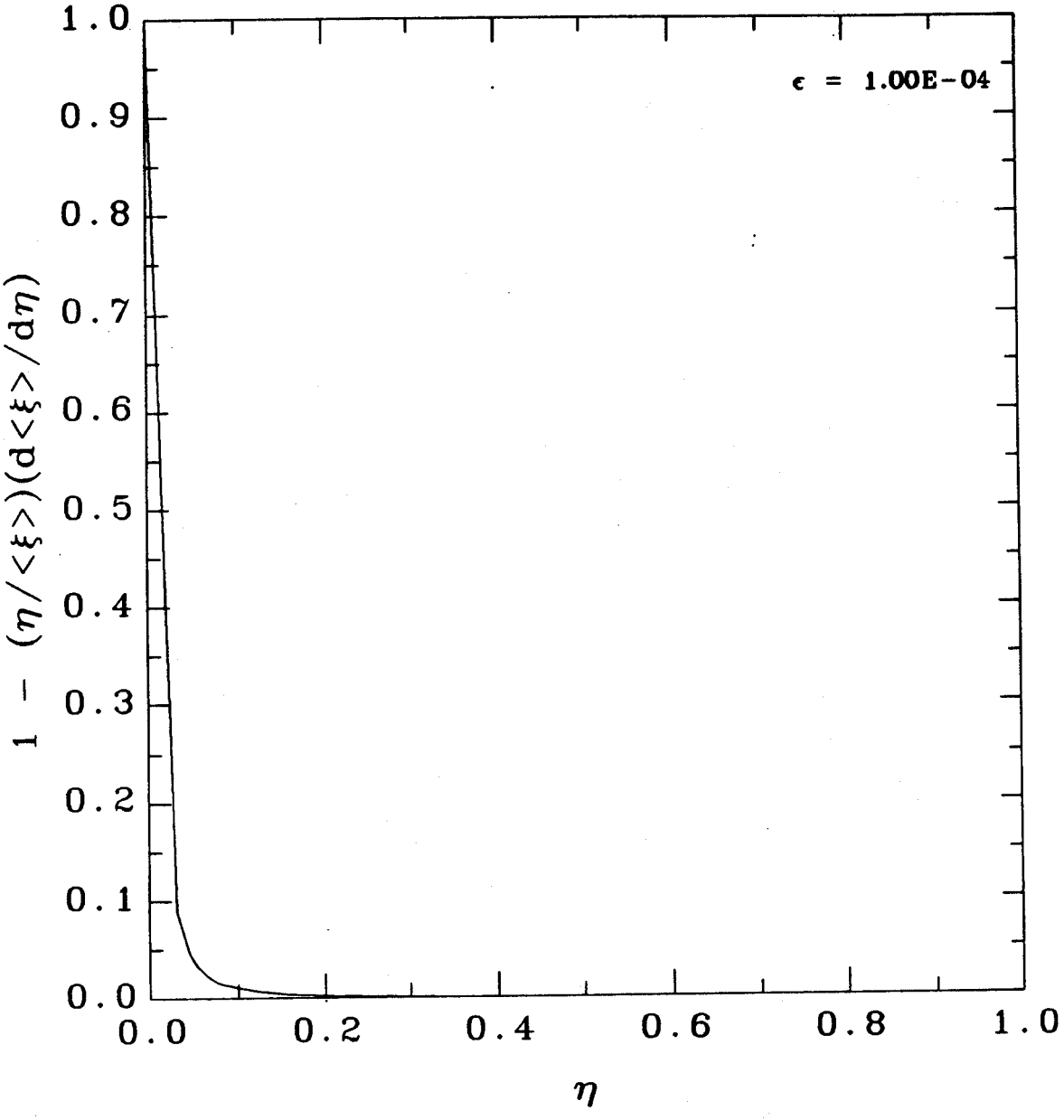

Fig. 4

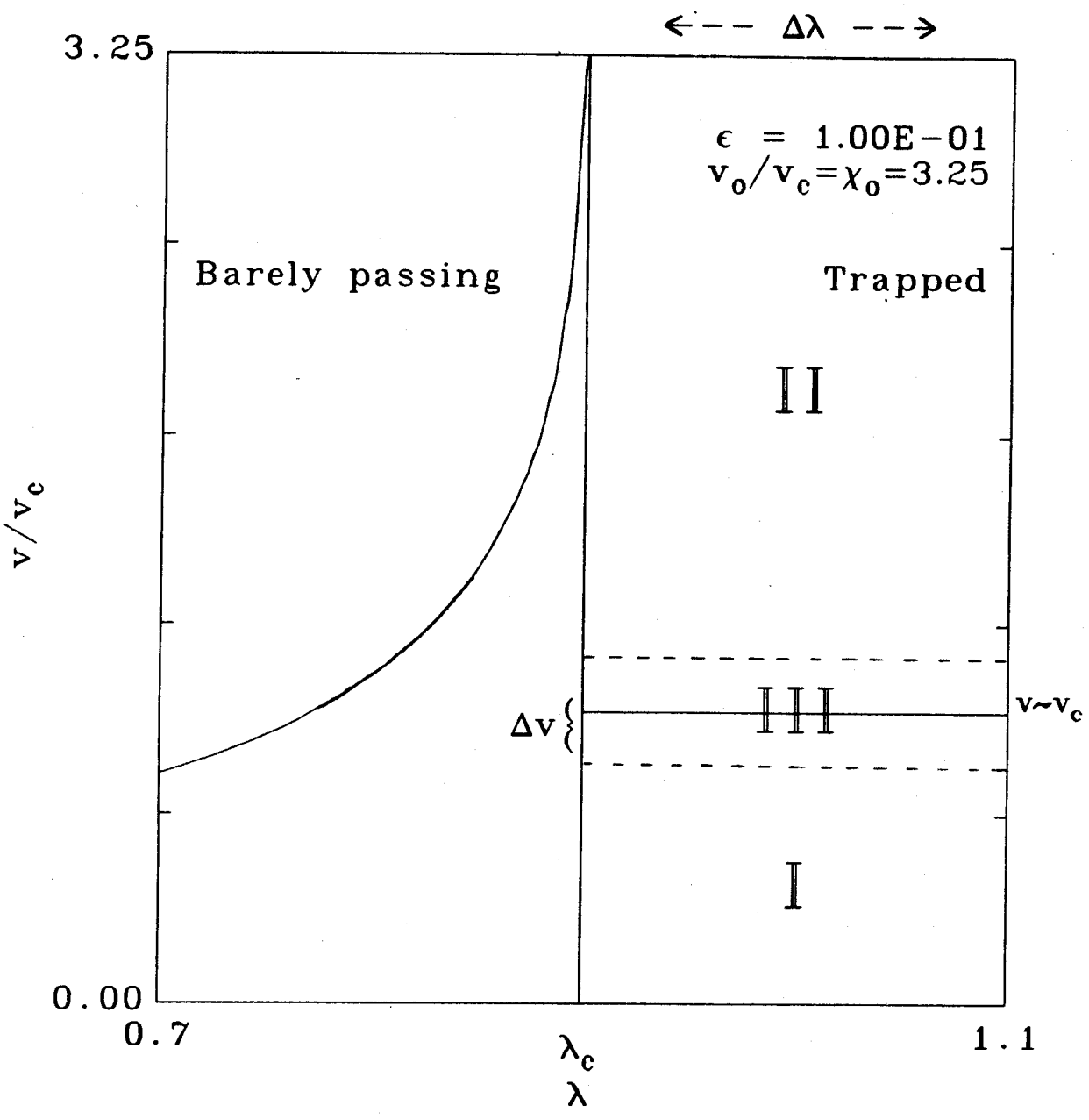
3.25
0.00
0.7
1.1
λ_c
λ
v/v_c
$\leftarrow\!-\!-\ \Delta\lambda\ -\!-\!\rightarrow$
ϵ = 1.00E-01
$v_0/v_c=\chi_0=3.25$
Barely passing
Trapped
II
III
I
Δv
$v\sim v_c$

Fig. 5